Nuclear Quantum Effects in Water and Aqueous Systems: Experiment, Theory, and Current Challenges

Michele Ceriotti[1], *Wei Fang*[2], *Peter G. Kusalik*[3], *Ross H. McKenzie*[4], *Angelos Michaelides*[2], *Miguel A. Morales*[5], *Thomas E. Markland**[6]

[1] Laboratory of Computational Science and Modeling, Institute of Materials, École Polytechnique Fédérale de Lausanne, 1015 Lausanne, Switzerland, [2] Thomas Young Centre, London Centre for Nanotechnology and Department of Physics and Astronomy, University College London, London WC1E 6BT, United Kingdom , [3] Department of Chemistry, University of Calgary, 2500 University Drive NW, Calgary, Alberta T2N 1N4, Canada [4] School of Mathematics and Physics, University of Queensland, Brisbane, 4072 Queensland, Australia [5] Lawrence Livermore National Laboratory, Livermore, California 94550, USA, [6] Department of Chemistry, Stanford University, 333 Campus Drive, Stanford, California 94305, USA

*****Email: tmarkland@stanford.edu

Abstract

Nuclear quantum effects influence the structure and dynamics of hydrogen bonded systems, such as water, which impacts their observed properties with widely varying magnitudes. This review highlights the recent significant developments in the experiment, theory and simulation of nuclear quantum effects in water. Novel experimental techniques, such as deep inelastic neutron scattering, now provide a detailed view of the role of nuclear quantum effects in water's

properties. These have been combined with theoretical developments such as the introduction of the competing quantum effects principle that allows the subtle interplay of water's quantum effects and their manifestation in experimental observables to be explained. We discuss how this principle has recently been used to explain the apparent dichotomy in water's isotope effects, which can range from very large to almost nonexistent depending on the property and conditions. We then review the latest major developments in simulation algorithms and theory that have enabled the efficient inclusion of nuclear quantum effects in molecular simulations, permitting their combination with on-the-fly evaluation of the potential energy surface using electronic structure theory. Finally, we identify current challenges and future opportunities in the area.

Contents

1. Introduction

Due to the low mass of the proton and the central role of hydrogen bonding Nuclear Quantum Effects (NQEs), such as Zero-Point Energy (ZPE) and tunneling, can play an important role in determining water's static and dynamical properties. Understanding these effects and developing methods to efficiently simulate them are thus vital to obtain a chemically accurate description of water's properties from simulations, and to elucidate experimentally observed static and kinetic isotope effects. While aspects of NQEs in water have been reviewed previously(1), there have been significant recent developments such as an improved theoretical understanding of their role in modulating hydrogen bond strengths, new algorithms to efficiently include them in simulations, and new experimental techniques to probe them.

In particular, the competing quantum effects picture has provided significant insights into the interplay between different NQEs in the hydrogen bond(2-7). This concept is based around the observation that NQEs lead to an extension of the Oxygen (O) – Hydrogen (H) covalent bond allowing the protons to be more shared (delocalized) between hydrogen bonded pairs of water molecules as shown in the left panel of Fig. 1. This effect acts to strengthen the hydrogen bond. However, quantum fluctuations also allow the protons to spread in the other directions, leading to distorted and hence weaker hydrogen bonds as shown in the right panel of Fig. 1. Which of these effects dominates is strongly determined by the distance between the oxygen atoms of the hydrogen bonded water molecules with short hydrogen bonds being made stronger upon the inclusion of NQEs while long ones are made weaker. This concept of "competing quantum effects", has been shown during the last decade to be a highly useful organizing principle to provide a much clearer understanding of the large variation in the magnitude of isotope effects observed in water(2, 4-6).

This theoretical picture has been coupled with new algorithms, which have greatly reduced the cost of performing simulations that include NQEs – in some cases yielding schemes with costs comparable to those of the corresponding classical simulation(8-16). These algorithmic advances have allowed simulations of liquid water with NQEs to be performed where the molecular interactions are computed using on-the-fly electronic structure calculations(5, 17-22) and on potential energy surfaces fit to high-level *ab initio* calculations(23-27). In addition, experimental techniques such as deep inelastic neutron scattering (DINS) are now able to probe the proton and oxygen momentum distributions and quantum kinetic energies, providing intriguing new observations of these quantum properties of the nuclei at thermodynamic conditions ranging from supercooled to supercritical water, and environments ranging from the bulk to hydrophobic confinement(26, 28-42).

Given the vast range of environments and aqueous systems in which NQEs can occur this review cannot hope to be comprehensive. Hence our focus in this review is to highlight some of the latest developments in the application of theory, modeling and experiments to NQEs in water and offer a perspective on how these developments will build into new discoveries in the future. First, we summarize experimental isotope effects observed in the static and dynamic properties of water with an emphasis on large and seemingly anomalous effects. Second, we discuss recent theoretical and simulation work that has allowed many of these effects to be elucidated. We then summarize methods for the efficient and accurate inclusion of NQEs in simulations to obtain static and dynamical properties of water. Finally, we summarize the ongoing challenges and opportunities that remain in understanding and modeling NQEs in water.

2. Experimental Observations of Nuclear Quantum Effects in Water

In this section, we provide a brief overview of various micro- and macroscopic properties of water that exhibit notable experimental isotope effects. In particular, we will emphasize that while many experiments suggest that NQEs act to weaken the hydrogen bond, leading to a less structured liquid and a more mobile hydrogen bonded network in H_2O than in the less quantum mechanical D_2O, this is not always the case, and can depend both on the conditions and the property of interest. Where appropriate in this section we included mention of relevant simulation work used to analyze the experiments. However, the bulk of the simulation work and the theoretical origins of water's seemingly ambivalent response to the inclusion of NQEs are covered in more detail in Sec. 3.

Isotope effects for a range of properties are summarized in Table 1 upon exchanging H for Deuterium (D) or Tritium (T), or ^{16}O for ^{18}O. While H_2O and D_2O data are available for many of water's properties in its numerous chemical phases, much more limited data is available for $H_2{}^{18}O$ and T_2O. We have included values for $H_2{}^{18}O$ where available, because it has the same molecular mass as D_2O thus allowing one to compare the influence of the molecular mass, which changes on $^{16}O/^{18}O$ substitution, and effects due to the moment of inertia and proton ZPE that change upon H/D substitution. At the outset it is interesting to note that water's seeming ambivalence to quantum effects for some properties is reflected in the fact that prokaryotic organisms such as bacteria can tolerate pure D_2O conditions(43), while deuterating about 30% of plant's and mammal's water can be lethal(44-46).

2.1 Energy Scales of Quantum Effects in Water

Isotope effects in water range from those observed at ambient conditions, which can often be attributed to the ZPE in the O-H stretch or other degrees of freedom, to those at high pressures

or low temperatures where tunneling and proton delocalization become particularly important(47-54). The ZPE of the O-H stretch is equivalent to a ~2000 K rise in temperature along that coordinate and is modulated by the local hydrogen bonded structure of water, for example in different phases, at interfaces or in the presence of solutes. At high pressures and/or low temperatures, the uncertainty in the proton's position becomes comparable to the distance between the minima in the potential energy surface. This can lead to proton tunneling and extensive delocalization that are strongly coupled to changes in the distances between oxygen atoms(2, 18, 55).

NQEs manifest as isotope effects upon substitution of H for D or T, or ^{16}O for ^{18}O. While it is common to view deuterated water as a "classical" analogue of water, it is important to note that although D_2O and T_2O have smaller NQEs, they are not classical species. The vibrational frequencies in Table 1 allow one to estimate that the ZPE in liquid water is ~21 kJ/mol per O-H stretch, and that the O-D and O-T stretches still possess ZPEs of ~15 kJ/mol and ~12 kJ/mol respectively, i.e. still ~71% and ~58% of that in H_2O. One can also estimate the total harmonic contribution to the zero-point energy in the gas phase to be ~54 kJ/mol for H_2O and ~40 kJ/mol for D_2O. These estimates give an idea of the energetic scale of NQEs at room temperature, as compared to the classical contribution to the (intramolecular) kinetic energy of 3.7 kJ/mol at 300 K. In addition, while $^{16}O/^{18}O$ substitution generally gives rise to small isotope effects, they are widely used in atmospheric isotope fractionation studies that form crucial inputs to climate modeling(56, 57).

2.2 Thermodynamic Properties

Gas phase properties of the water molecule are shown in Table 1. The covalent bond energies exhibit a quantum effect, with the O-D bond being about 1.6% stronger than the O-H bond. This amounts to a difference of 7.5 kJ/mol which is largely accounted for by the difference in the O-H and O-D ZPEs of 5.8 kJ/mol. D_2O has essentially the same gas phase dipole moment as H_2O, which is perhaps not unexpected given that their bond length and angles are almost identical (less than 0.05% difference in both cases)(58). However, D_2O has a dimer dissociation energy that is about 12.7% larger than H_2O, suggesting D forms a substantially stronger hydrogen bond than H in the gas phase. In addition, the relative stabilities of the low temperature structures of the water hexamer have also been shown to be highly sensitive to NQEs(59-61).

A number of observations suggest that the stronger hydrogen bond observed for D_2O in the gas phase is also present in the liquid. For example, the melting point is increased by 3.82 K upon deuteration, which is indicative of the idea that D forms a stronger hydrogen bond that leads to an increase in the stability of ice over the liquid. The temperature of maximum density (TMD) is increased by 7.21 K upon deuteration and hence the difference between the melting point and TMD increases from 3.73 K to 7.37 K, indicating that a universality scaling to the TMD is insufficient to account for these isotope effects. The effect of NQEs and isotope substitution on the melting point(62-64), TMD(4, 63) and phase diagram of water(65) has been quite well reproduced theoretically through simulations using the q-TIP4P/F water model. The heat capacity for the liquid is also considerably larger for D_2O than for H_2O at a given temperature (see Table 1), and recent work of Vega and coworkers has highlighted that this is a reflection of the importance of NQEs in water even at ambient conditions(66). Comparison of the molar densities, both at the temperature of maximum density and at 298 K, reveals a small contraction for D_2O and T_2O, and a small expansion of $H_2{}^{18}O$. Although it may be tempting to

interpret these changes in density as suggesting stronger hydrogen bonding in the more dense D_2O and T_2O, one should be careful since due to the directional nature of hydrogen bonds stronger hydrogen bonding can lead to decreased density (e.g. as observed in simulations based on Kohn-Sham Density Functional Theory (DFT) with the Generalized Gradient Approximation (GGA) descriptions of water(67)). The pH of liquid water is also increased from 7.0 to 7.4 upon deuteration and rises to 7.6 upon tritiation(68, 69). This data is consistent with a quasiharmonic scaling that predicts that the pK_a varies as the inverse square root of the particle mass(8). Given this relation one can extrapolate to the classical (infinite mass) limit which implies that the pH of "classical" water would be ~8.5; i.e. a ~30-fold change in the acid dissociation constant.

All of these observations are broadly consistent with a picture that NQEs weaken the hydrogen bond in liquid water and therefore that the hydrogen bond is strengthened upon deuteration. However, other properties are not consistent with such an interpretation. For example, the critical temperatures of D_2O and T_2O are lower than those for H_2O, suggesting that at these higher temperatures NQEs act to strengthen hydrogen bonds – in contrast to the observed behavior at lower temperatures. Comparison of the liquid/vapor surface tension also indicates a seemingly anomalously smaller value for D_2O relative to H_2O.

With H/D substitution the volume of liquid water and of ice Ih increases by 0.1%. This increase is anomalous as many liquids and solids exhibit a volume decrease upon substitution with a heavy isotope(70). Furthermore, the magnitude of the change for water is anomalously small for a hydrogen bonded compound. Figure 2 shows experimental data for the change in O-O bond length with H/D substitution for a wide range of compounds. This is referred to as the secondary geometric isotope effect. The primary geometric isotope effect refers to changes in the O-H bond lengths. Figure 2 also compares the experimental results with the predictions based on

the simple diabatic state model discussed in Sec. 3.4(2). Of particular note is that for liquid water and ice Ih the effect (~0.001 Å) is relatively small, highlighting that the competing quantum effects in water under these conditions almost exactly cancel. Similar results and conclusions have been obtained from path integral molecular dynamics (PIMD) simulations as discussed below(70).

2.3 Spectroscopic Properties

X-ray spectroscopies(71, 72) that probe the local structure in liquid water have provided further evidence that D_2O makes stronger hydrogen bonds than H_2O at room temperature. X-ray Raman Scattering (XRS)(71) experiments have been used to compare the structure of H_2O and D_2O at different temperatures, revealing that the structure of H_2O at a lower temperature appears similar to that of D_2O. XRS, X-ray Absorption Spectroscopy (XAS)(73-75) and X-ray Emission Spectroscopy (XES)(76-78) have been used to propose and probe the balance of two structural classes of hydrogen bonds, tetrahedral and asymmetric, in liquid water. By comparing the XRS(71) spectroscopic features assigned to the asymmetric species, it was observed that H_2O's asymmetric hydrogen bonds show enhanced asymmetry compared to D_2O. This asymmetry is present even when the effect of an offset in temperature was taken into account. In addition, comparing the vibrationally resolved spectra for H_2O, D_2O and HDO(72) using resonantly excited XES in which asymmetrically hydrogen bonded molecules (with one strong and one weak/broken hydrogen bond in the HDO liquid) were selectively excited, a strong preference was observed for OD as the strong and OH as the weak/broken hydrogen bond. A ratio as high as 1.5(±0.2):1 was found compared to the 1:1 ratio that would be expected for classical water(72). Hence, the common practice in femtosecond pump-probe vibrational spectroscopies, where

dilute HDO in either H_2O or D_2O is probed on the assumption that the OH and OD stretches probe the same hydrogen bond situations with equal statistical weight, is challenged when NQEs are considered.

The concept that D_2O is a more structured liquid than H_2O at ambient temperatures is also supported by X-ray, γ-ray and neutron scattering experiments(79-81). These studies indicate a general broadening of structural features in going from heavy to light water where the Radial Distribution Functions (RDF) for liquid D_2O appears slightly more structured, characterized by more pronounced peaks in the O-O RDF as shown in Fig. 3, than those for liquid H_2O with the O-H covalent bond being longer than the O-D bond by as much as ~3%(80). In turn the hydrogen bond is shorter by ~4%, the first intermolecular OH peak is more asymmetric, and the first HH intermolecular distance is ~2% longer, in H_2O compared to D_2O(80). However, other neutron scattering results using oxygen substitution and using a different analysis technique(82) have suggested the covalent bond length change upon deuteration to be significantly smaller at around 0.5%(83, 84). Hence there still remain significant uncertainties in the experimental difference between the RDFs for light and heavy water. The enhanced hydrogen bonding asymmetry in H_2O compared to D_2O deduced from XRS(71) is thus further supported by the combined X-ray and neutron scattering data(80).

2.4 Dynamical Properties

Data on how isotopic substitution affects the dynamical properties of water are also listed in Table 1. In particular we report information on the translational diffusion, rotational diffusion, the dielectric relaxation time, and the (dynamic) viscosity. These are all also consistent with D having a stronger hydrogen bond at around 300 K with the mobility of D_2O about 20-30% lower

than that of H_2O. The rise in the viscosity of 23% upon deuteration is accompanied with a fall in diffusion of 23%, consistent with Stokes-Einstein behavior. It is important to note that isotope substitution gives rise to bigger proportional changes in the dynamical properties than those observed for most static properties. This is partially since dynamical events are driven by rare fluctuations in the hydrogen bond network that are altered much more by quantum effects than the average value of the properties. However, it is also because even in the classical limit changing H to D results in a change in the dynamics, unlike static equilibrium properties, due to the increase in the mass. This trivial contribution, which does not arise from NQEs, results in a slowing of dynamical properties upon substituting H for D. This slowing ranges from a factor of $(m_H/m_D)^{1/2}$=0.707 if the dynamical process arises from pure ballistic motion of the substituted atom, to $(m_{H2O}/m_{D2O})^{1/2}$=0.949 if the process involves ballistic motion of the center of mass of the water molecule. Notably, NMR experiments(85) show that at higher temperatures (around 573 K) the translational diffusion constants for D_2O and H_2O undergo an apparent crossover (i.e. their ratio drops below the expected change of 0.949).

2.5 Tunneling and Proton Delocalization Effects

At low temperatures or when water molecules are forced into close proximity (such as at high pressure or at interfaces), more pronounced quantum effects can occur, arising from proton tunneling and delocalization. In particular, experimental and theoretical studies on high pressure ice have shown quantum tunneling of protons in ice VII(47, 51) while higher pressure ices such as ice X exhibit symmetric hydrogen bonds, where the protons are located halfway between two water molecules(51, 86, 87). The adsorption of water on solid surfaces is an area that has received considerable attention from the surface science community(88-90) and on some

surfaces water molecules can be forced into close proximity because of their interaction with the substrate. The shortened distances between neighboring molecules can then lead to quantum proton delocalization(91), as shown for example through scanning tunneling microscopy (STM) experiments of water clusters on Cu(110)(92) on Au-supported NaCl(001) films where it was possible to directly probe concerted proton tunneling in water tetramers(93).

2.6 Solvation Properties

It is also worth briefly commenting on the effect that NQEs have on changing the solvation behavior of species. For the solvation of large biomolecules(94, 95), small molecules(96-98), and ions(99) small changes have been observed in the dynamics, solvation free energy and structure surrounding them upon including NQEs. Indeed, in experiments on gas phase HOD hydrogen bonded complexes with fluoride and iodide ions the former ion binds preferentially to OH and the latter to OD(99). This inversion of behavior for ions that strongly and weakly bind water further suggests a delicate cancellation between different NQEs. A recent simulation study has suggested that there is an absence of notable NQEs in the solvation of monovalent ions, such as Li^+ and F^-, due to competing quantum effects (see following section)(100) although another recent study treating the water molecules as rigid entities, and hence neglecting competing quantum effects, observed the hydrogen bond dynamics of water around F^- to be nearly 40% faster than observed in classical simulations(101).

When light species, such as solvated protons(102-107), hydroxide(108, 109), hydrogen atoms(110, 111) and electrons(112-120), which themselves exhibit notable NQEs, are solvated in water larger effects are often observed. For example NQEs reduce the free energy barrier to bulk proton transfer by a factor of ~3(121, 122). Experimentally proton diffusion has been observed to

be slowed by a factor of ~1.5 upon deuteration(123). Hence the excess proton in water diffuses ~4.1 times faster than water itself whereas D^+ diffuses faster by only a factor of ~3.6 in D_2O. Hydrogen atom and muonium (Mu), an isotope of hydrogen with approximately one-ninth the mass, diffusion has also been studied in liquid water and hexagonal ice both by experiment(124-126) and simulation(110, 111). In room temperature water little change in the diffusion constant is observed upon changing the atom from Mu to H. This has been explained by considering the effective swelling of the water cavity which holds the Mu atom due to the zero-point pressure exerted by the quantum particle on the water(110). This behavior leads to a turnover where at temperatures above ~300K Mu diffuses faster than H whereas below that temperature, both in the liquid and in hexagonal ice, H diffuses faster. At very low temperatures where tunneling dominates Mu is again observed to diffuse faster than H(124).

2.7 Absolute Measures of Nuclear Quantum Effects

While the change of the aforementioned properties upon isotope substitution provide an indication of the role of NQEs, even tritiated water is far from the classical limit, making it hard to assess their total contribution. Properties for which the classical limit can be predicted exactly are therefore particularly interesting as they give an absolute measure of NQEs.

For instance, the logarithm of the equilibrium isotope fractionation of hydrogen and deuterium between liquid water and its vapor would be zero if the nuclei were classical particles(6). These water fractionation ratios are used to provide a means of monitoring spatial and historical variation in atmospheric temperatures(57). For example, fractionation ratio measurements from Antarctic ice cores are used to provide information about global

temperatures over the past 300,000 years(127). Figure 5 shows the fractionation ratio plotted as 1000 $\ln(\alpha_{l\text{-}v})$ where $\alpha_{l\text{-}v}$ is defined as

$$\alpha_{l-v} = \frac{(x_{D,l} / x_{H,l})}{(x_{D,v} / x_{H,v})} = e^{-\Delta A/k_B T}$$

where x_Z is the mole fraction of isotope Z, *l* denotes the liquid phase, and *v* denotes the vapor phase. ΔA is the Helmholtz free energy corresponding to the process,

$$H_2O_{(l)} + HOD_{(v)} \rightleftharpoons H_2O_{(v)} + HOD_{(l)} \ .$$

Hence a positive value ($10^3 \ln \alpha > 0$) corresponds to a preference for H to reside in the gas phase compared to D and a negative value for it to reside in the liquid phase. If hydrogen bonds formed by D in the liquid are stronger than those formed by H, then one would expect an excess of D in the liquid, where hydrogen bonds can be formed, compared to in the gas, where they are not. Isotope fractionation ratios can also be shown to be directly related to the quantum kinetic energy difference between the isotopes(6, 8, 128, 129).

As shown in Fig. 5 at room temperature experimentally (blue line) $10^3 \ln \alpha$ is positive, indicating a preference for D to reside in the liquid which suggests that it forms a stronger hydrogen bond. However, as the temperature is raised above 493 K the sign of $10^3 \ln \alpha$ inverts indicating that H is preferentially found in the liquid phase. This inversion, which can be explained by the competing quantum effects principle, provides another example that water exhibits a dichotomy in its NQEs under different conditions. As we will discuss in Sec. 3.2 the ability to model this effect is highly sensitive to the anharmonicity of the O-H stretch in the potential energy surface used.

DINS experiments can be used to provide measurements of the quantum kinetic energy and momentum distributions of protons, deuterons and more recently heavier nuclei(130). In the classical limit the total kinetic energy of a nucleus reduces to its classical equipartition value

($3k_BT/2$) and the momentum distribution is simply the Maxwell-Boltzmann distribution. However, due to the quantum nature of nuclei, both quantities vary depending on the environment, and can be related to the shape of the potential experienced by the nucleus(14, 35, 42, 47, 131-134). DINS measurements thus rely on the quantum nature of nuclei to extract valuable information on the structure and behavior of light atoms in the condensed phase. These experiments have now been performed extensively on bulk water at different points of its phase diagram(28-30, 32-36, 38, 134) and have suggested that protons in confined water exhibit an anomalous excess of kinetic energy(37).

In addition by measuring the different components of the kinetic energy tensor in different phases, DINS provides perhaps the most direct experimental probe of competing quantum effects. Specifically, Romanelli et al.(30) found that the principal values of this tensor changed in opposite directions when heavy-water ice melts. This significantly reduces the net quantum effect on the kinetic energy change, and can be related to the relatively small net quantum effect on the melting temperature. These experimental results agree qualitatively with PIMD simulations using potential energy surfaces from DFT(30).

3. Simulations and Theory of Nuclear Quantum Effects in Water

In this section, we summarize some recent insights that have been obtained from simulations of water. Increases in computational power and improved algorithms to include NQEs in simulations (discussed in Sec. 4) have led to a major surge of activity including applications to systems ranging from bulk liquid water to water at surfaces. This has also enabled various comparisons with experiment to be made and given insight into properties that are not directly

observable by experiment. Performing such calculations with different computational approaches has also made it possible to assess the reliability of different models.

3.1 The Structure of Bulk Liquid Water

Early path integral simulations of liquid water using empirical potentials employed rigid water molecules or described the O-H stretch using a purely harmonic potential. These studies appeared to show a consistent picture that NQEs weaken the hydrogen bond network in water leading to a less structured (lower and broader) first peak in the O-O RDF(135-138), which is broadly consistent with the experimental refinement of neutron and x-ray scattering data show in Fig. 3. To produce an equivalent change in the RDF by changing the temperature in a classical simulation required about a 35-40 K increase.

However, a study using a flexible empirical water model that included anharmonic terms in the O-H stretch revealed that this was an incomplete picture(4). Upon including the anharmonicity, the ZPE allows the proton involved in the hydrogen bond to extend in the direction of the acceptor oxygen to form a stronger hydrogen bond. This counterbalances the weakening effect, resulting in a smaller total impact of NQEs. These competing quantum effects, first observed in water, have since been extended to explain a much wider range of hydrogen bonded systems using *ab initio* PIMD(7) (which exactly include NQEs on static properties for a given potential energy surface as discussed in Sec. 4). This work revealed a general trend that weak hydrogen bonds are weakened by NQEs while strong hydrogen bonds are strengthened by NQEs(7). Behind this trend is the competition between the NQEs in librational modes and the NQEs in stretching modes, where in relatively weak hydrogen bonds, the former dominate, and in relatively strong hydrogen bonds, the latter dominate.

The extent of this cancellation of NQEs in water however has remained a matter of debate since it depends sensitively on the electronic structure approach or force field used to model the water interaction – in particular as to the anharmonicity of the O-H coordinate. For example competing quantum effects were also hinted at in an earlier study using DFT(5) but a subsequent simulation using the same exchange-correlation functional suggested this was not the case(17). Due to the pioneering nature of these early path integral calculations the total time run in both of these simulations was less than 20 ps (including equilibration). Hence statistical error bars are likely to be an issue in detecting the subtle differences that occur in the O-O RDF upon inclusion of NQEs. However, due to the recent introduction of algorithms to efficiently include NQEs (14, 139) and current computational power it has now become possible to perform simulations long enough to exhaustively sample the O-O RDF using *ab initio* PIMD simulations. Fig. 4 shows the results obtained from two recent studies using two different GGA functionals at 300 K. The quantum and classical nuclei RDFs shown in 4(a) were each obtained from 100 ps of dynamics using the recently introduced *ab initio* ring polymer contraction scheme(139) (see Sec. 4.1.4) while those in 4(b) were obtained from 150 ps of classical parallel tempering followed by 100 ps of simulation using the PIGLET(14) algorithm (see Sec. 4.1.3). In both cases the qualitative changes to the RDF are consistent. Namely in the first coordination shell the rise in the first peak occurs at a slightly shorter distance which is complemented by a lowering of the first O-O peak height (integration of the quantum and classical RDF's to obtain the coordination number in the first shell indicates that, in both cases, the coordination number is essentially unchanged). The minima following the first peak of the RDF is deeper in the quantum case for both functionals followed by a slightly higher second peak, which suggested increased structure in the second coordination shell. Inspection of the 3D distribution function in 4(c) for the BLYP

exchange correlation functional allows one to pinpoint the origin of the increased structure of the second peak: interstitial configurations, corresponding to distorted H-bond geometries become less abundant in the presence of NQEs, with an increase in density in the region at about 4 Å corresponding to the second neighbor in ice Ih. This destabilization of interstitial defects may explain the counter-intuitive structure-enhancing effect of quantum delocalization. However, despite the consistency of these two GGA functionals as to the influence of NQEs on liquid water's structure more accurate descriptions of its electronic structure may alter this balance.

While there is undoubtedly a degree of cancellation of different quantum effects on the O-O RDF, quantum effects on individual H-bond coordinates can be dramatic. The fluctuations of a proton along the covalent bond direction increase almost tenfold relative to a classical simulation. It was observed that, as a consequence of quantum fluctuations, protons in liquid water experience transient excursions bringing them closer to the acceptor than donor oxygen atom(18, 19). Analysis of the electron densities (by means of maximally localized Wannier functions) (140) showed that these extreme quantum fluctuations are stabilized by considerable electron density rearrangements. However, the number of these excursions in liquid water remains a matter of debate since different DFT exchange-correlation functionals predict that these events occur for between 0.5% and 0.05% of the protons in water at a given time(18, 19).

Quantum fluctuations along the hydrogen bond direction can also favor genuine autoprotolysis, and transition to delocalized-proton, super-ionic states. PIMD simulations of liquid water at 10GPa and 750 K, where the density is 65% higher than that of the ambient liquid, also show frequent proton exchanges between water molecules when NQEs are included. A similar interplay of pressure-induced delocalization and nuclear quantum fluctuations has been shown in action in exotic phases of ice at low temperature(47, 141).

3.2 Isotope Fractionation as a Probe of Nuclear Quantum Effects

To try and clarify the nature and impact of the competing quantum effects concept, a number of recent theoretical studies have concentrated on the ability of models to accurately obtain the H/D isotope fractionation ratio between liquid water and its vapor. As discussed in Sec. 2.7, the logarithm of this ratio would be zero in a classical simulation and is thus a very direct probe of NQEs since it is known very accurately under NVT conditions from experiments(6, 8, 18). The isotope fractionation ratio can be shown to relate directly to the quantum kinetic energy of the protons in water. Hence by decomposing the quantum kinetic energy in a molecular reference frame(6, 131, 142), one can observe the contribution of its different components. The different components of the kinetic energy of heavy water near its melting point have been obtained from DINS experiments and *ab initio* PIMD results using the BLYP functional showed good agreement with the experimental data(30).

Based on this line of thinking, it was possible to show using PIMD simulations that the anharmonic flexible q-TIP4P/F model(4), which was the model originally used to suggest the existence of competing quantum effects in water, is able to accurately obtain the correct fractionation ratio over a wide range of temperatures(6) as shown in Fig. 5 (red line). Moreover it even accurately reproduced the experimental temperature where the fractionation ratio inverses, indicating that temperature affects the two competing quantum effects differently and hence can change their balance. This is in contrast to rigid and harmonic models, such as the harmonic q-SPC/Fw potential in Fig. 5 (black line), which considerably overestimate the extent of fractionation compared to experiment and give no inversion point. By projection of the kinetic energy into the internal molecular coordinates it was shown that the component of the

fractionation arising from the O-H stretch undergoes a large cancellation (~90%) with the contribution of the in-plane and orthogonal librations. This example highlights that one must be careful when simulating quantum effects with force fields, since many force fields are parameterized to properties of chemical bonds near their equilibrium bond lengths. However due to the large amount of ZPE a quantum particle may explore a much larger part of the potential energy surface, where the force field may not be accurate. For example, the TTM3-F model which was fit to high level *ab initio* calculations(24) shows a qualitatively incorrect inverted fractionation behavior at room temperature. This arises since the slope of the TTM3-F dipole moment surface at large O-H bond extensions increases the charge on the H too much upon hydrogen bonding(6). This leads to the dominance of hydrogen bond strengthening upon including quantum effects and hence the incorrect inverted fractionation behavior at room temperature. The more extreme O-H bond lengths that lead to this failure are however extremely rare in classical simulations, which lack the ~21 kJ/mol of ZPE in that coordinate, and hence TTM3-F fares much better in classical simulations.

Recent developments in methods to efficiently include NQEs(14) and simulate isotope effects(8, 129, 143, 144) have also allowed the assessment of these effects in properties such as the fractionation ratio when combined with an on-the-fly evaluation of the potential energy surface using a variety of DFT exchange-correlation functionals. Since treating competing quantum effects requires an accurate description of a much wider range of the potential energy surface, it is a sensitive probe as to whether an electronic structure method is able to correctly reproduce the behavior of hydrogen bonded systems. For example, recent work has studied the isotope fractionation of water with *ab initio* path integral simulations(18), to assess the role of including exact exchange and van der Waals corrections on the PBE and BLYP functionals. The

PBE functional was shown to overestimate the contribution of the O-H stretching and predicted inverted isotope fractionation to experiment at room temperature ($10^3 \ln\alpha$=-17) while the BLYP functional ($10^3 \ln\alpha$=62) agreed much better with experimental values ($10^3 \ln\alpha$=73) and correctly reproduced the inversion observed in the experimental fractionation (Fig. 5 – green line), albeit predicting the inversion to occur at too low a temperature. Including some exact exchange in the PBE functional (PBE0) improved the overestimation of NQEs in the O-H stretching coordinate and gave the correct qualitative behavior at 300 K ($10^3 \ln\alpha$=90). It was also shown that the magnitude of the fractionation ratio predicted was highly correlated with the number of "proton excursions" observed in path integral simulations of the functional.

In addition, to assess the ability of DFT to reproduce hydrogen bond structures when NQEs are included another recent study benchmarked the energy of configurations in bulk water obtained from a variety of DFT exchange-correlation functionals against quantum Monte Carlo, which provides a highly accurate benchmark(145). When the configurations were obtained from a PIMD simulation GGA functionals gave energy errors about twice as large as for hybrids. However, when the configurations were taken from a classical MD simulation much smaller differences were observed between GGAs and hybrids. This is because quantum fluctuations allow the O-H atoms in a covalent bond to sometimes come closer, and GGAs tend to predict these bonds to be too soft in water(146, 147). Due to the local nature of this problem adding exact exchange(147) or a monomer correction to DFT(148) can somewhat alleviate this problem of the internal O-H covalent bonds in the water molecule.

3.3 Water at Interfaces

The quantum nature of water at interfaces and under confinement has been examined in a number of recent simulation studies (see e.g. Refs. (91-93, 122, 149-154)), sometimes also with a view to understanding related experiments. These have started to reveal evidence under certain circumstances for quite strong quantum effects including tunneling, proton delocalization and hydrogen bond symmetrization. We do not attempt a comprehensive review of the literature in this very interesting area, but rather focus now on one particular area where strong evidence for such effects has been obtained. Specifically we talk now about the adsorption of water on metal surfaces. Various experiments and simulations(89, 90) provide evidence to suggest that in some adsorption systems rather short O-O separations can be obtained. This comes about because on metal surfaces water molecules generally bind preferentially above individual metal atoms of the substrate(155); for close-packed surfaces of metals with relatively small lattice constants molecules at adjacent sites can therefore be in close proximity. On the (111) surface of Ni, for example, this can in principle lead to O-O separations as short as 2.5 Å. With this in mind Li *et al.*(91) performed a series of *ab initio* PIMD simulations for water overlayers on several metal surfaces (Ni(111), Ru(0001), and Pt(111)). The particular overlayers considered were mixtures of water and hydroxyl molecules that form on many metal surfaces when e.g. water and oxygen are coadsorbed(90). Fig. 6 reports some of the key results of that study for the structures of the overlayers formed on the three surfaces. Specifically distributions of O-H and O-O bond lengths show that as one goes from the substrate with the largest lattice constant considered (Pt) to the one with the smallest (Ni) the degree of hydrogen bond symmetrization increases. In some situations on Pt and Ru HO-H-OH-like complexes are observed (Fig. 6(g)) whereas on Ni protons are almost perfectly shared between neighboring molecules (Fig. 6(h)).

Direct experimental evidence for hydrogen bond symmetrization has yet to be obtained for the specific overlayers probed in Ref. (91). However, evidence for a very closely related adsorption structure comprised of a single H_2O and a single OH has been obtained by means of STM on the (110) surface of copper(92). In an elegant set of highly controlled experiments, Kumagi et al. managed to observe the formation of a water-hydroxyl complex out of individual coadsorbed water and hydroxyl molecules. The complex that formed had a symmetric oval shape and along with complementary DFT calculations it was argued that the oval image was evidence for the formation of an HO-H-OH-like complex with the H between the two oxygens shared symmetrically. In this particular case the ZPE level along the hydrogen bond sits quite a bit above the very small potential energy barrier for proton transfer along the O-O axis. Kumagai et al. have also performed a number of similar studies of related adsorption systems and much of this has been reviewed recently(156). Amongst other things this work has revealed clear experimental evidence of hydrogen bond exchange in adsorbed water clusters(152) in support of earlier theoretical predictions(150).

3.4 A Simple Diabatic Model of NQEs in the Hydrogen Bond

As discussed, while many properties suggest water becomes less structured upon increasing NQEs by replacing D with H. However, other properties, particularly those at higher temperatures suggest the opposite trend. The concept of competing quantum effects provides an organizing principle to understand this behavior as well as a range of other phenomena in hydrogen bonded systems(2, 5, 7). Figure 1 shows two hydrogen bonded water molecules and highlights the vibrational modes that are of particular relevance for a single O-H bond: the stretch, a bend in the plane of the water molecule, and a bend out of the plane of the water

molecule. A key property of hydrogen bonding is that the frequencies of these modes vary significantly with the distance R between the oxygen atoms. Furthermore, as R increases the hydrogen bond between the molecules becomes weaker causing stretch modes to stiffen and the bend modes to soften(2).

The physics of these competing quantum effects is captured within the potential energy surface (PES) given by a recently introduced simple model for hydrogen bonding based on two electronic diabatic states(3). The two states differ by transfer of a proton, and the model is similar in spirit to Empirical Valence Bond models(157-161). It uses only two free parameters; they describe the energy and length scale associated with the coupling of the two diabatic states. The key descriptors are the proton-donor acceptor distance R (i.e. the separation between the oxygen atoms) and the difference ε between the proton affinity (or equivalently pK_a) of the donor and the acceptor. The model gives a ground state PES, $E(R,r,\varphi)$ where r is the length of the O-H bond in the donor molecule and φ is the deviation of the hydrogen bond from linearity (as depicted in Fig. 1). If one uses this surface to calculate the classical (harmonic) stretch and bend vibrational frequencies one finds that as R increases the stretch frequency increases and the bend frequency decreases, with associated change in their ZPE in opposite directions. This competition between the stretch ZPE, which favors stronger and shorter hydrogen bonds, and bend ZPEs, which favors longer and weaker ones, is the essence of competing quantum effects in hydrogen bonded systems.

Despite its seeming simplicity this model of the hydrogen bond and its competing quantum effects describes a wide range of experimental observations, from bond lengths to vibrational frequencies, including both primary and secondary isotope effects. For example, the observed correlation with R of both the O-H stretch and the out of plane bending frequencies, for

a wide range of compounds, is quantitatively described by this model(2). Indeed, in going from the gas phase to liquid water the OH stretch frequency is measured experimentally to decreases from 3657 to 3404 cm^{-1}(162, 163). In contrast, the OH (in-plane) bend frequency increases from 1595 to 1644 cm^{-1}. This clearly shows competing quantum effects: hydrogen bonding decreases the ZPE associated with stretch and increases that of the bend vibrations. This is also seen in high pressure experiments on ice VIII: with increasing pressure the frequency of the stretch modes decreases and those of the librational modes increase(164, 165). In addition, as shown in Fig. 2(b) this model also captures the dependence of the H/D secondary geometric isotope effect on the O-O distance, R for a wide range of compounds.

4. Methods to Simulate Nuclear Quantum Effects

NQEs must be included in any atomistic simulation that aims at capturing the whole spectrum of properties of systems that contain light atoms. In molecules or in solids they can often be modeled accurately using a harmonic or quasi-harmonic approximation. However, in liquids such as water, it is necessary to fully account for anharmonic and entropic effects, requiring a more comprehensive treatment of NQEs.

One of the most promising approaches to include NQEs in the static equilibrium properties of anharmonic systems are techniques based on the Feynman path integral formulation of quantum mechanics(166, 167), which can be used in conjunction with Monte Carlo(168-170) or molecular dynamics(171-174) to treat exactly the quantum statistics of an ensemble of distinguishable nuclei. It will be evident already from the discussions in Sec. 3 that these techniques have found widespread use; mainly this is due to the combination of effective algorithms that have reduced their computational cost combined with increases in computational

power. In Sec. 4.1, we provide a brief introduction to path integral methods along with specific comments and recommendations about their application to liquid water. We will only consider distinguishable particles since nuclear exchange is expected to play a minor role in the description of liquid water since the two spin states, ortho and para water are closely degenerate in gas phase which we expect to carry over also to the condensed phase(175). For a detailed discussion of path integrals for bosons and fermions we direct the reader to review articles focusing on that topic(168, 176).

We will then address the techniques that can be used to approximate the effects of NQEs on time-dependent properties. Due to the challenge of real time quantum dynamics, which is formally exponentially scaling in both time and dimensionality, currently no method exists that allows one to obtain exact results for complex condensed phase systems such as water. Nonetheless, significant progress has been achieved in the area of semi-classical quantum dynamical methods in the last decade and a discussion of these approaches will be presented in section 4.2.

4.1 Simulating Quantum Static Properties

Imaginary time path integral methods represent the most convenient framework to introduce NQEs in atomistic simulations to obtain static equilibrium properties. The path integral representation is based on the general expression for the expectation value of an operator:

$$\left\langle \hat{O} \right\rangle = \int d\vec{R} \left\langle \vec{\mathrm{R}} \middle| \hat{\rho} \middle| \vec{R} \right\rangle O(\vec{R})$$

where $\hat{\rho}$ is the density operator which, for simplicity, we assume is diagonal in configuration space. In the case of the canonical ensemble, which we consider here (generalization to other ensembles is straightforward), the density operator takes the form $\hat{\rho}=e^{-\beta \hat{H}}$. Using the simple

property that the product of density matrices is a density matrix, $e^{-(\beta_1+\beta_2)\hat{H}} = e^{-\beta_1\hat{H}}e^{-\beta_2\hat{H}}$, the expectation value can be rewritten as a path integral:

$$\left\langle \hat{O} \right\rangle = \int \left[\prod_{i=1}^{P} d\vec{R}_i \ \left\langle \vec{\mathrm{R}}_{\mathrm{i}} \left| \mathrm{e}^{-\tau \hat{\mathrm{H}}} \right| \vec{R}_{\mathrm{i+1}} \right\rangle \right] \ \frac{1}{\mathrm{P}} \sum_i O(\vec{R}_i),$$

where $\tau = \beta / P$. This expression is exact for any value of P, it merely replaces the density matrix at an inverse temperature β with a product of P density matrices at the smaller inverse temperature τ. Since there are no known analytic expressions for the density matrix of an arbitrary Hamiltonian at finite inverse temperature, we must resort to approximate expressions in practical calculations. In almost all cases, the approximations employed are exact in the limit $\tau \to 0$, which means that computed quantum averages are exact in the limit of infinite P and convergence to this limit must be carefully assessed in all calculations. Approximate expressions typically offer a trade-off between the speed of convergence with P and the complexity of the expression (computational, ease of implementation, robustness, etc.). In the following, we discuss the main alternatives used in practical calculations and their relevance to the study of liquid water. In addition, we try to offer useful advice about their use when possible.

4.1.1 Second-Order Approximation: Also known as the primitive approximation, this is the simplest and most common approximation to the short-time thermal density matrix. It is based on the Trotter expansion(177),

$$e^{-\tau\hat{H}} = \left(e^{-\tau/2\hat{V}} e^{-\tau\hat{T}} e^{-\tau/2\hat{V}} \right) e^{O(\tau^2)}$$

and is correct to order $O[\tau^2]$. It is particularly convenient as it leads to a classical Hamiltonian that is isomorphic to a "ring polymer" composed of P copies of the system, with corresponding

atoms connected by harmonic springs as shown in Fig. 7. P is referred to as the number of polymer beads. This form allows the partition function to be sampled by Monte Carlo (PIMC) or Molecular Dynamics (PIMD), using similar algorithms that can be used for the corresponding classical simulation. While this approach only requires the evaluation of energies and forces for the P replicas, and properties converge to the quantum limit with increasing P, the convergence is rather slow. In the case of water at ambient conditions P=32 is typically used for calculations with flexible water monomers which is enough to obtain reasonably converged properties like the quantum kinetic and potential energies and RDFs(4, 15, 135, 178). Other quantities might converge at a slower rate. For example in the case of liquid water, converging the heat capacity to reasonable accuracy at ambient conditions typically requires P~128(15, 179, 180). The second-order approximation is the most common implementation of PIMD and is the one employed in most software packages that offer PIMD as an option. However, as discussed below, in many cases its efficiency can be enhanced by combining it with techniques such as reweighting, colored noise thermostats or ring polymer contraction based approaches.

4.1.2 Higher-Order Approximation: In order to improve the speed of convergence of path integrals with P, the use of higher-order approximations to Trotter's expansion have been investigated in detail over the last decades. As discussed by several authors(181-184), the use of higher-order approximations (beyond second-order) invariably leads to nested commutators of the kinetic and potential energy, which in turn lead to complicated operators that are hard to evaluate in practice for general potentials. Even the simplest of these expansions, proposed by Takahashi and Imada(185), contains a term proportional to the square modulus of the force acting on the atoms. While its use in PIMC methods is possible, its use in PIMD is limited since

the derivative of this term in the Hamiltonian needed to generate the dynamics to sample the phase space requires calculating the first-order derivatives of the force, *i.e.* the Hessian matrix. Hence, for most potentials, any gain obtained by an improved convergence of properties with P is typically lost by the much more costly evaluation of the Hessian. For this reason, higher-order approximations to the thermal density matrix have been used only sporadically.

An interesting alternative to the use of high-order expansions in PIMD is the use of re-weighted estimators(16, 186, 187). In this case, estimators derived from a high-order approximation are evaluated using a re-weighting procedure with trajectories obtained from second-order PIMD calculations. This avoids the need for Hessian matrices if they do not appear in the estimators themselves, since the trajectories are propagated using the simple Trotter PIMD Hamiltonian. While this scheme has been shown to lead to reduced efficiency as the system size grows with the benefit becoming negligible around 100 water molecules(188), it can be extremely useful for smaller systems when extremely accurate convergence of NQEs is required.

4.1.3 Accelerated Path Integrals with Generalized Langevin Equations: Generalized Langevin equations (GLE) have recently been suggested as highly tunable thermostats in classical MD simulations(189, 190), and have been extended to non-equilibrium thermostat schemes that can be used to mimic nuclear quantum fluctuations in quasi-harmonic systems(191, 192). Furthermore, it has been shown that a combination of path-integral molecular dynamics and generalized Langevin equations (PI+GLE) can be conceived, which for harmonic systems yields virtually exact structural properties with any number of replicas, and is guaranteed to converge to Trotter path integrals in the limit of large P[15] (since in this limit the effect of the non-equilibrium GLE disappears leaving the standard second order expression). Since the GLE term effectively

guarantees convergence of the harmonic terms, only anharmonicities need to be recovered directly by increasing the number of beads, leading to a dramatic reduction in the number of replicas required for convergence. This idea was later extended to also provide accurate estimates for momentum-dependent observables, such as the quantum kinetic energy (PIGLET)[16]. For example, as shown in Fig. 8, for liquid water at ambient conditions, PIGLET with P=6 already leads to well-converged properties. The additional computation necessary to implement the PIGLET thermostat is small compared to the evaluation of the forces in most systems, leading to a negligible overhead. PIGLET is thus currently one of the most effective approaches to incorporate NQEs in the calculation of static properties.

4.1.4 Ring Polymer Contraction: Another alternative to accelerate the cost of converging PIMD calculations is the use of the Ring Polymer Contraction (RPC) approach(11-13). The main idea of RPC, which shares some similarities with the ideas behind multiple time-step algorithms in classical MD simulations(193), is to break up the interaction into stiff and soft components, and use the Trotter expansion in such a way that the stiff components, such as chemical bonds, are evaluated with a smaller value of τ. This can be easily seen in the following partitioning of the density matrix:

$$e^{-\tau\hat{H}} \approx e^{-\tau/2\hat{V}_{soft}} \left(e^{-\tau/2n\hat{V}_{stiff}} e^{-\tau/n\hat{T}} e^{-\tau/2n\hat{V}_{stiff}} \right)^n e^{-\tau/2\hat{V}_{soft}} .$$

In this case, the stiff interaction is evaluated *n* times more than the soft interaction. Since the soft component is slowly varying in space compared to the stiff component, it can then be evaluated on a contracted ring polymer, consisting of fewer beads $P'=P/n$, with negligible loss in accuracy. If the stiff component is chosen such that it can be evaluated much more quickly than the soft component, which is only evaluated P' times, then one can substantially decrease the cost of the

calculation. One of the main benefits of this idea is that it can be combined with almost any other PIMD approach, including those presented above, leading to dramatic improvements in the efficiency of path integral simulations. The main challenge is the need to divide the interaction into stiff and soft contributions. In the case of liquid water at ambient conditions, using a an empirical water potential(4), RPC makes it possible to evaluate the intra-molecular part of the potential on the full P=32 ring polymer, while the expensive long-range electrostatic interactions can be computed just once, on the centroid.(12, 13) RPC approaches are thus highly appealing to use whenever possible and have been implemented in the i-PI program(194) and the Graphical Processing Unit (GPU) accelerated OpenMM code(195, 196). Owing to the need to separate the time-scales present in the potential energy, the application of RPC to *ab initio* PIMD simulations has provided more of a challenge. However, recent work has shown that RPC can be used to dramatically accelerate both DFT(139) and MP2(197) calculations, while retaining chemical reactivity, by using a reference potential to create a smooth difference force which can then be evaluated on the contracted ring polymer.

4.1.5 Other approximations: The approximations discussed above represent formally exact methods in the limit of infinite P. As long as one is careful in testing convergence with P, exact quantum averages can be obtained for any interaction type and strength. Other methods exist that lead to approximate results, but typically at reduced computational cost and complexity. The simplest of these approaches is the use of perturbation theory to obtain quantum corrections to classical averages such as the Wigner-Kirkwood formula(198, 199). It is worth noting that many of these approaches can be easily derived from the path-integral formulation and are associated to the re-weighted estimators discussed above when used in combination with classical

simulations instead of second-order expansions. Another closely related approach is the use of Feynman-Hibbs effective potentials and similar ways to incorporate NQEs approximately through renormalized interactions(166, 200). These schemes are typically based on the use of high-order expansions for the thermal density matrix to construct corrections to the interactions that can be used in an otherwise classical simulation. A very recently introduced approach along these lines is to use the expansion of the free energy in orders of ħ (Planck's constant) to obtain a correction to the second-order path integral partition function for a given P(201). This perturbed path integral approach was shown to accelerate the convergence of the energy of liquid water with convergence achieved at P=6 compared to the usual value of P=32.

It is also worth mentioning that a number of studies have attempted to account for NQEs in water by increasing the temperature of an otherwise classical simulation, for example the use of classical results at higher temperatures as a means to reproduce quantum results at T=300 K(202). This idea can be seen as a "poor man's" version of the most primitive form of a quantum GLE (Sec. 4.13), which is based on the idea of simulating ZPE by enforcing a frequency-dependent effective temperature on different normal modes(191). However, the use of a uniform, modified classical temperature misses the strong anisotropy of the quantum momentum distribution, and can only reproduce a subset of the quantum properties. Furthermore, in hydrogen bonded systems, such as water, that exhibit strong competing quantum effects, even the properties that appear correct may be reproduced for the wrong reason, and will be strongly dependent on the model chosen to describe inter-atomic forces. For example: the temperature shift required to replicate NQEs for the single property of the change in the first peak of the O-O RDF of room temperature liquid water was shown to range from 5 K to 40 K depending on the water model chosen(84) and one would expect different DFT exchange correlation functionals to

show similar varaibility(18). Hence even for a single property the effective temperature change needed to account for NQEs can vary wildly(203).

Hence, while these more *ad-hoc* approaches eliminate altogether the need for multiple replicas, and are therefore as inexpensive as a classical simulation, they do so at the expense of introducing uncertainties that are difficult to quantify. This is particularly worrisome in a system such as water that involves significant molecular anisotropy and a competition of NQEs along different molecular axes. Considering the availability of efficient and systematically converging techniques such as the PIGLET and RPC we expect the need to such approximate approaches will be much decreased in the future.

4.2 Simulating Quantum Dynamical Properties

When it comes to including NQEs in simulations of dynamical (time-dependent) properties the currently tractable computational techniques are much less reliable. In the case of gas-phase aqueous systems and small clusters, high-end benchmark calculations exist(204, 205), that demonstrate the dramatic effects of quantum coherence on the very low-temperature vibrational spectrum of hydrogen-bonded systems. Unfortunately, since the cost of these exact methods grows exponentially with the dimensionality of the problem, one has to resort to approximate methods to treat the condensed phases of water. In the study of chemical reactions at very low temperature quantum instanton techniques(206) provide a robust framework to include ZPE and tunneling effects on reaction rates, but they are not easily extended to room temperature and the liquid state. In practice, the techniques that have been used more often to approximately describe quantum dynamics in water can be roughly classified in two different classes.

One class of methods treat a subset of the degrees of freedom quantum mechanically, embedding this quantum subsystem into the bulk environment which is treated as static or as evolving in time according to classical dynamics. This family of techniques includes those based on the semi-classical theory of lineshapes(207), that have been used with great success to model the response of an isolated chromophore in water, comparing successfully with experimental techniques ranging from simple infra-red absorption(208) to more sophisticated spectroscopies(209). Another possibility is to use the local monomer approximation (LMon), that is based on selecting a subset of the local normal modes of one water molecule, computing the variations of the potential energy and the dipole moment as a function of the distortion of the molecule along these coordinates, and solving the Schrödinger equation for these modes in a fixed electrostatic environment(210, 211).

The other classes of methods treat the whole system on equal footing, but heavily approximate the underlying nuclear dynamics. These methods typically utilize imaginary-time PIMD trajectories (Sec. 4.1) to construct initial configurations consistent with quantum statistics, from which approximate trajectories are then initiated to calculate the relevant time correlation function for the dynamical property of interest. Linearized semi-classical initial value representation methods use Newtonian dynamics to evolve these trajectories in time(212-215), which in the case of liquid water has been shown to be seriously affected by issues arising from unphysical ZPE leakage(216). Very recently, a modified formulation of this approach, Matsubara dynamics, has been introduced that preserves detailed balance and might help formulate more rigorous approximations of quantum dynamics(217, 218).

Another possibility involves the use of modified forms of PIMD to generate approximate real-time correlation functions. Ring polymer molecular dynamics (RPMD) simply evolves the ring

polymer according to the discretized path integral Hamiltonian(9, 219-221), while centroid molecular dynamics (CMD) approximates the centroid-density dynamics by evolving the center of mass of the ring polymer over the potential of mean force obtained by averaging over the internal fluctuations of the ring polymer(222-224). Both techniques can be shown to yield exact quantum dynamics in some simple limiting cases, and some progress has been made towards giving formal justification to their use(217, 225, 226). In general they can be expected to be more reliable for the evaluation of quantum corrections to long-time dynamical properties (*e.g.* diffusion coefficients). CMD and RPMD have been used to study diffusion and rotational relaxation in neat water(4, 135, 227), and CMD has been applied together with a multi-state empirical valence bond potential to study the dynamics of the excess proton in bulk water(104). However, both methods have been shown to exhibit serious artifacts when used to compute properties that are related to non-linear operators and high-frequency vibrations(228-235). The latter problem can be mitigated by attaching thermostats to the internal modes of the ring polymer, a technique that can be seen as being half-way between RPMD and CMD(236). In fact, one can see that as long as one avoids stepping outside of each method's comfort zone, CMD and thermostated RPMD give results that are consistent with each other and with methods based on a quantum description of a subset of the degrees of freedom(236). NQEs are indispensable if one wants to achieve a quantitatively-accurate description of the dynamical properties of water, but the differences between the various methods are comparable to those one should expect from performing simulations on an imperfect potential energy surface.

4.3 Computational Infrastructure and Codes to Include Nuclear Quantum Effects

One of the aspects that hinder more widespread modeling of NQEs in simulations of water arises from the technical complexities of performing a path-integral simulation - particularly in conjunction with a first-principles solution of the electronic structure. A few major codes for atomistic simulations provide some implementation of PIMD(195, 196, 237-243), but often these implementations do not cover the whole spectrum of techniques discussed in this review, or are not very actively maintained. A possible solution to this issue could come from a more modular design of the codes. A very convenient feature of PIMD is that the technicalities of the implementation do not involve a tight coupling with the internal workings of how inter-atomic forces within each replica are computed. Hence, it is possible to separate the details of path-integral methods and those of the force calculation, and develop a library of full-fledged PIMD routines that simply rely on one of the existing atomistic simulation packages to compute energy and forces for a given configuration of the atoms. i-PI is a recently-developed package that implements this idea in a radical way, using inter-process communication and a client-server design, so that any electronic structure or force field code can be easily patched to act as an energy and force back-end to quantum simulations of nuclear statistics and dynamics(194). The same idea could be realized in a more closely integrated manner whenever the force back-end provides a standardized library interface.

5. Outlook and Ongoing Challenges

The past decade has seen some significant advances in our characterization and understanding of NQEs in water. The challenge of the next decade will be to exploit these advances to provide a complete picture of water's NQEs in all regions of its phase diagram, in particular the deeply supercooled regime where these effects might be expected to be particularly important, as well as

in its solvation properties and in broken symmetry environments such as interfaces and in confinement. These environments can require longer time-scales and larger system sizes to simulate and have thus proved elusive but with recent developments are now within reach. It will be interesting to see how the competition between quantum effects in water is mediated by such environments. Finally, below we highlight three areas which we believe are essential to develop in order to obtain a more complete understanding of NQEs in water.

5.1 Experiments

DINS has revealed the momentum distribution of protons, and can be compared to path integral simulations(17, 30, 34, 47, 132, 134). Furthermore, this has illuminated competing quantum effects(2, 4, 7, 30). However, there remains some ambiguity associated with interpreting the DINS experiments. Going from the data to robust (i.e. non-controversial) spatial probability distributions for protons, particularly ones involving proton delocalization needs to be improved.

In addition, new experiments that have probed isotope effects in deeply supercooled water have shown divergences between the static length-scales in D_2O and H_2O as well as a series of other intriguing observations(35, 73). Given that a number of quantum effects have been demonstrated in the dynamics of other glassy quantum systems arising from quantum ZPE "swelling" it will be interesting to see if these play a role in supercooled water(244, 245).

5.2 Potential Energy Surfaces

Path integral simulations will only be as good at the potential energy surfaces that they use. NQEs such as tunneling are particularly sensitive to the energy barrier for proton transfer. For example, we described work that shows how calculated isotope effects vary significantly with

the DFT exchange-correlation functional that is used. This is because the potential energy surface, particularly with respect to the proton transfer co-ordinate, is quite sensitive to the oxygen-oxygen separation, and to the level of quantum chemical theory. For example for $H_3O_2^-$ the PBE functional predicts a shared symmetric proton even in classical MD simulations whereas more accurate simulations using second order Møller-Plesset perturbation theory (MP2) or the BLYP functional show that the protons actually exhibit a double-well potential(7). This becomes particularly important for properties that are determined by rare events (i.e. thermal and quantum fluctuations to short hydrogen bonds). The development of new DFT exchange correlation functionals and the ability to use hybrid functionals(202, 246, 247) with van der Waals corrections(146, 248-250) offers one such opportunity. In addition recent developments in electronic structure theory and ongoing increases in computational power have made simulations using MP2 theory possible for condensed phase water(251) while recent algorithms have also improved its scaling(252). For small gas phase molecules higher-level methods, such as coupled cluster theory, can also be utilized with PIMD simulations(253). In addition recent simulations of liquid water using highly accurate quantum Monte Carlo surfaces suggest that PIMD simulations of this kind might soon become practical(254). New accurate intermolecular potential energy surfaces, such as MB-pol, also present new opportunities for identifying more accurately the role of NQEs in pure water(27, 255-257).

5.3 Methods and software to efficiently include nuclear quantum effects

The combination of advanced path integral algorithms with ongoing significant increases in computational power and the exploitation of novel computational architectures such as GPUs(55, 258-260), now allow *ab initio* PIMD simulations on condensed phase aqueous systems of 100s

of atoms to be performed on a fairly routine basis. This, combined with the wider availability of codes to perform such calculations will extend our ability to obtain much more detailed sampling and to reach the system sizes needed to simulate liquid water at interfaces with other materials. Owing to the larger range of hydrogen bond strengths and hence modulation in the ZPE, in these environments one might expect to see pronounced NQEs. These developments will also allow simulations to reach the time-scales needed to start to probe the role of quantum effects in more slowly relaxing environment where rare-events, which are often greatly enhanced by NQEs, give rise to relaxation.

The ability to treat the quantum *dynamics* of aqueous system however still remains elusive and although methods like CMD and RPMD can be easily applied to aqueous systems and appear to give reliable results for properties such as diffusion constants, rates and reorientation times their performance on infra-red spectra leaves cause for concern. It will be interesting to see if the new generation of ensemble conserving linearized path integral methods such as the Feynman-Kleinert Quasi-Classical Wigner method(261), Path Integral Liouville Dynamics(262) or Matsubara dynamics(218) will yield more accurate results for such properties when directly applied to water or if they may yield directions as to how to improve existing methods such as RPMD and CMD.

Acknowledgements

We thank Lars G. M. Pettersson, Lu Wang and Ondrej Marsalek for providing insightful comments and suggestions for this review. This review was initiated during the Nordita (Nordic Institute for Theoretical Physics) scientific program “Water - the Most Anomalous Liquid”. Additional financial support for this program was provided by the Royal Swedish Academy of

Sciences through its Nobel Institutes for Physics and Chemistry, by the Swedish Research Council and by the Department of Physics at Stockholm University. M.C. acknowledges funding from CCMX and from the Swiss National Science Foundation (project ID 200021-159896). P.G.K is grateful for the financial support of the Natural Sciences and Engineering Research Council of Canada. A.M. and W.F.'s work is supported by the European Research Council under the European Union's Seventh Framework Programme (FP/2007-2013)/ERC Grant Agreement No. 616121 (HeteroIce project). A.M. is also supported by the Royal Society through a Wolfson Research merit Award (A. M.). M.A.M was supported by the Predictive Theory and Modeling for Materials and Chemical Science program by the Basic Energy Science (DOE-BES), and by the U.S. Department of Energy at the Lawrence Livermore National Laboratory under Contract DE-AC52-07NA27344. T.E.M was supported by the U.S. Department of Energy, Office of Science, Office of Basic Energy Sciences under Award Number DE-SC0014437. T.E.M also acknowledges support from a Cottrell Scholarship from the Research Corporation for Science Advancement and an Alfred P. Sloan Research fellowship.

Tables

Table 1. Experimentally observed isotope effects in water. Values for H_2O and D_2O, as well as T_2O and $H_2{}^{18}O$ when data is available, are compared. The values given are at 25 ˚C unless otherwise stated, and the values in parentheses are % shifts relative to H_2O.

Property	**H_2O**	**D_2O**	**T_2O**	**$H_2{}^{18}O$**	**Reference**
Bond energies (kJ/mol) (gas phase)	458.9	466.4 (1.6%)			(263)

Dipole moment (Debye) (gas phase)	1.855	1.855			(264)
Vibrational freq. (cm^{-1}) (gas phase)	3657.1 1594.7 3755.9	2671.6 1178.4 2787.7	2237.2 995.4 2366.6	3649.7 1588.3 3741.6	(162, 163)
Water dimer dissociation energy (kJ/mol) (gas phase)	13.22	14.88 (12.7%)			(265-267)
Melting point, T_m (1 atm)	273.15 K	276.97 K (1.40%)	277.64 (1.64%)	273.46 (0.11%)	(68, 69, 163)
Temperature of Maximum Density	277.13 K	284.34 K (2.60%)	286.55 K (3.40%)	277.36 K (0.08%)	(268, 269)
Critical temperature	647.10 K	643.85 K (-0.50%)	641.66 K (-0.84%)		(68, 163)
Molar density	55.35 mol/L	55.14 mol/L (-0.38%)	55.08 mol/L (-0.49%)	55.42 mol/L (0.13%)	(68, 270)
Molar density at TMD	55.52 mol/L	55.22 mol/L (-0.53%)	55.17 mol/L (-0.63%)	55.59 mol/L (0.13%)	(68, 269)
Liquid/vapor surface tension (N/m)	0.07198	0.07187 (-0.15%)			(68)
Specific heat capacity, C_v	74.54	84.42 (13.2%)			(68, 271)

(J/(K mol))					
Translation diffusion ($Å^2$/ps)	0.230	0.177 (-23.0%)		0.219 (-6.1%)	(272-274)
Rotational diffusion (rad^2/ps)	0.104	0.086 (-17%)			(275)
Dielectric relaxation time @20 ˚C (ps)	9.55	12.3 (29%)			(276)
Viscosity (mPa s)	0.8904	1.0966 (23.2%)		0.9381 (5.4%)	(68, 269)
Acidity pH / pD	7.00	7.43	7.6		(68, 69)

Figures

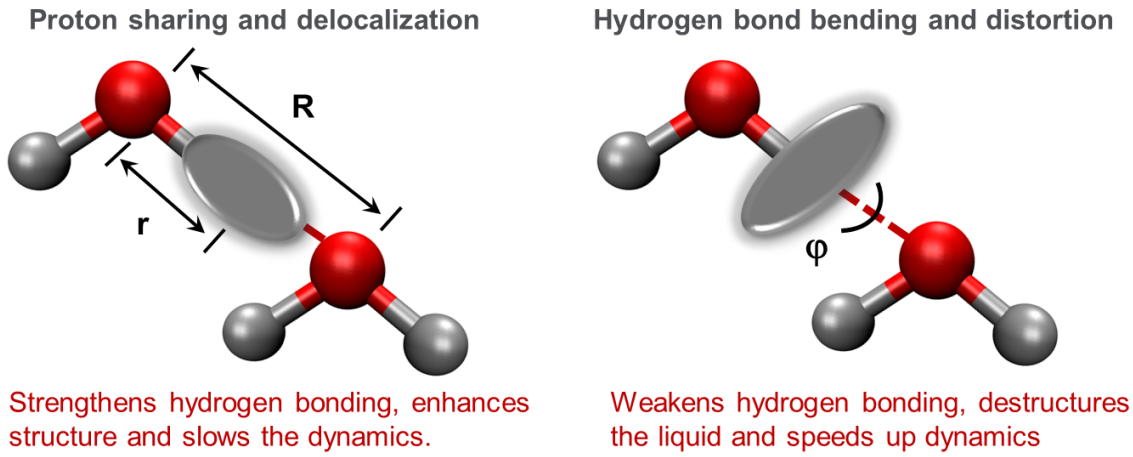

Figure 1. Competing quantum effects in the hydrogen bonding between two water molecules. There are two qualitatively different contributions to the vibrational ZPE. One is associated with the O-H stretch, shown on the left. The second contribution comes from the two bending vibrational modes: one in the plane of the water molecule, shown on the right, and the other perpendicular to the plane. As the distance, R, between the oxygen atoms decreases the stretch contribution decreases and the bend increases. Consequently, the two contributions respectively strengthen and weaken the hydrogen bond.

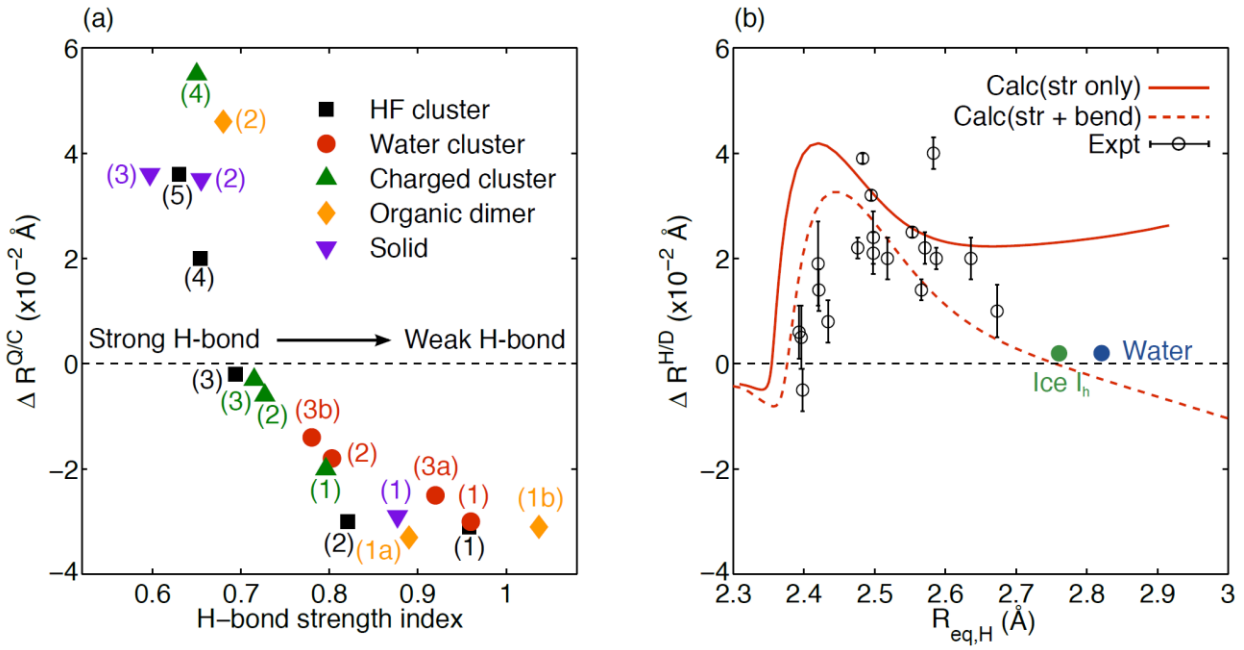

Figure 2. Secondary geometric NQEs in H-bonds. (a) Differences between the heavy-atom distances (R) in a H-bond from MD (with classical nuclei) and PIMD simulations (with quantum nuclei) (R^C-R^Q) vs. H-bond strength (defined as the ratio of the X-H stretching frequency in the H-bonded cluster to that in the free monomer). A positive value means that the H-bond is shorter when NQEs are incorporated. For the HF clusters, labels 1–5 refer to the H-bonds in the dimer to the hexamer. For the water clusters, labels 1, 2, 3a, and 3b refer to the H-bonds in the dimer, pentamer, and the long (short) H-bond in the octamer. For the charged clusters, labels 1–4 refer to H9O5-, H9O4+, H7O4- and H2H5- respectively. For the organic dimers, labels 1a, 1b, and 2 refer to the redshifted and blueshifted H-bond in formamide and the H-bond in formic acid. For the solids, labels 1–3 refer to the H-bonds in HCl, HF, and squaric acid. This figure has been adapted from Ref. (7) (b) Dependence of the secondary geometric isotope effect on the O-O distance R. This refers to the change in the O-O distance with H/D substitution (R^D-R^H). Experimental data for a range of different compounds is compared to the magnitude calculated from the simple diabatic state model(2, 3). The solid curve is the prediction when only the ZPE

of the O-H stretch is taken into account and the dashed curve when the O-H bend modes are also taken into account. Note that for weak hydrogen bonds the effect changes sign, i.e. weak hydrogen bonds get stronger with H/D substitution. This figure has been adapted from Ref. (2) (Copyright 2014 AIP Publishing). This figure illustrates how in water the overall NQE is relatively small due to competing quantum effects.

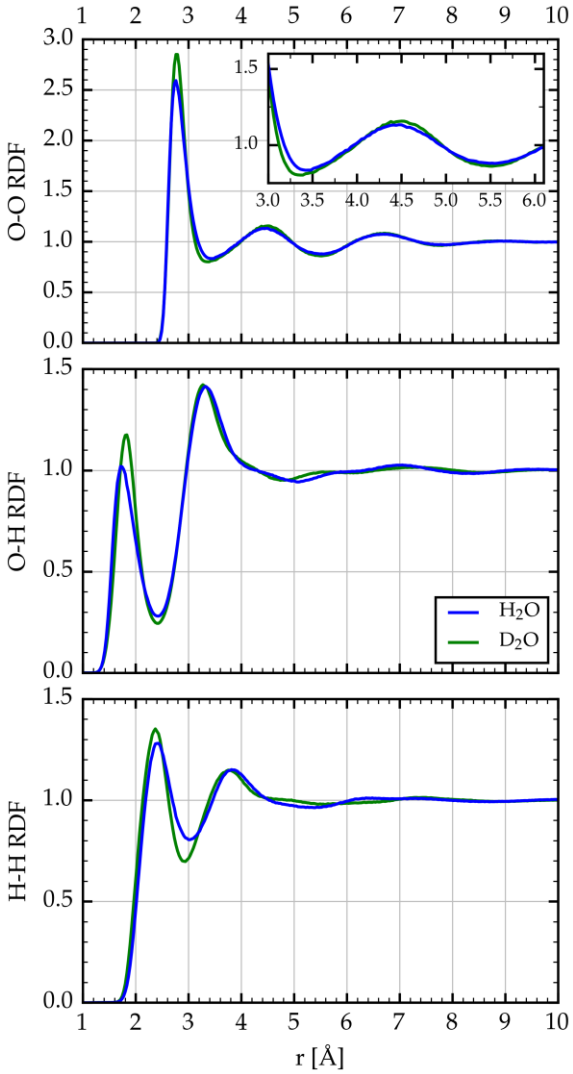

Figure 3. Radial distribution functions of liquid water for H_2O (blue line) and D_2O (green line) at 296 K obtained from refinement of neutron and x-ray scattering experiments. D_2O has a higher

first peak in the O-O radial distribution function suggesting it forms a more structured liquid. This figure was created from the data in Ref. (80).

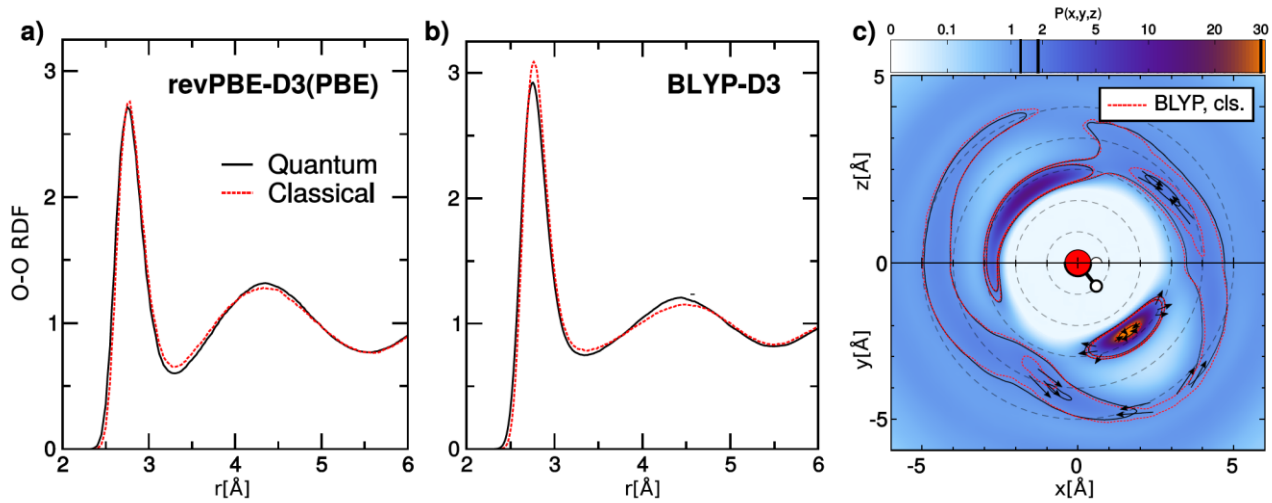

Figure 4. Radial distribution functions obtained from *ab initio* molecular dynamics simulations of liquid water at 300K, including nuclear quantum effects (black line) or with classical nuclei (red line). Panel (a) shows the results for revPBE functional with the PBE D3 vdW corrections (revPBE-D3(PBE)) obtained from a 100 ps simulation using *ab initio* ring polymer contraction. Panel (b) reports results obtained for BLYP with D3 vdW corrections (BLYP-D3) using a 150 ps classical parallel tempering run from which four independent quantum trajectories of 25 ps using six beads and PIGLET thermostatting were launched (a total of 100 ps of PIMD following the classical equilibration). Panel (c) reports slices of the 3D O-O distribution function along the plane of the molecule (*xy*) and the perpendicular plane (*xz*), for BLYP-D3; the color scale and the black contours correspond to the simulations with quantum nuclei, and the red dashed contours corresponds to the same density values but refer to a classical simulations. Arrows highlight the changes in probability distribution triggered by including NQEs.

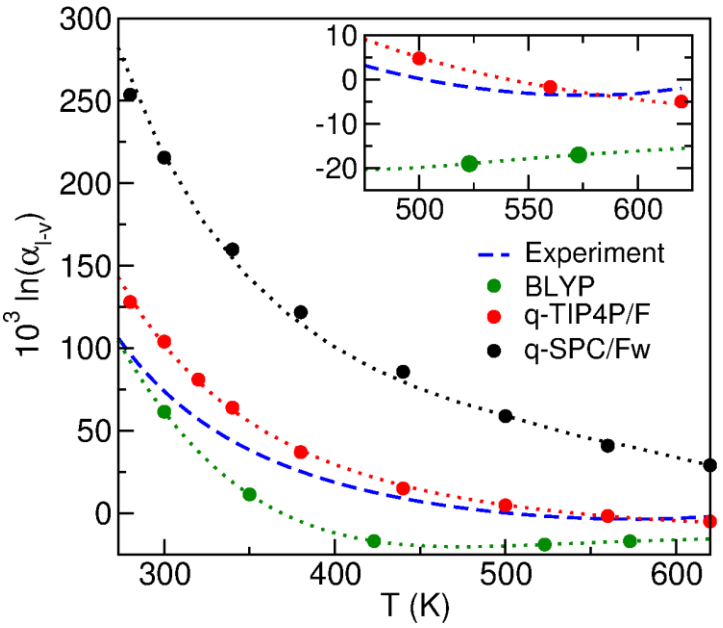

Figure 5. Liquid-vapor isotope fractionation ratio versus temperature from experiment(277) and theory(6, 18). Variation in the temperature corresponds to moving along the liquid-vapor coexistence curve. In the temperature range shown (up to 600 K) the density of the liquid phase changes by a factor of ~3. Hence, there is a significant variation in the O-O distance, and the strength of the hydrogen bonding. Around 500 K the experiments show an inversion in the fractionation ratio indicating D is preferentially found in the gas phase above that temperature.

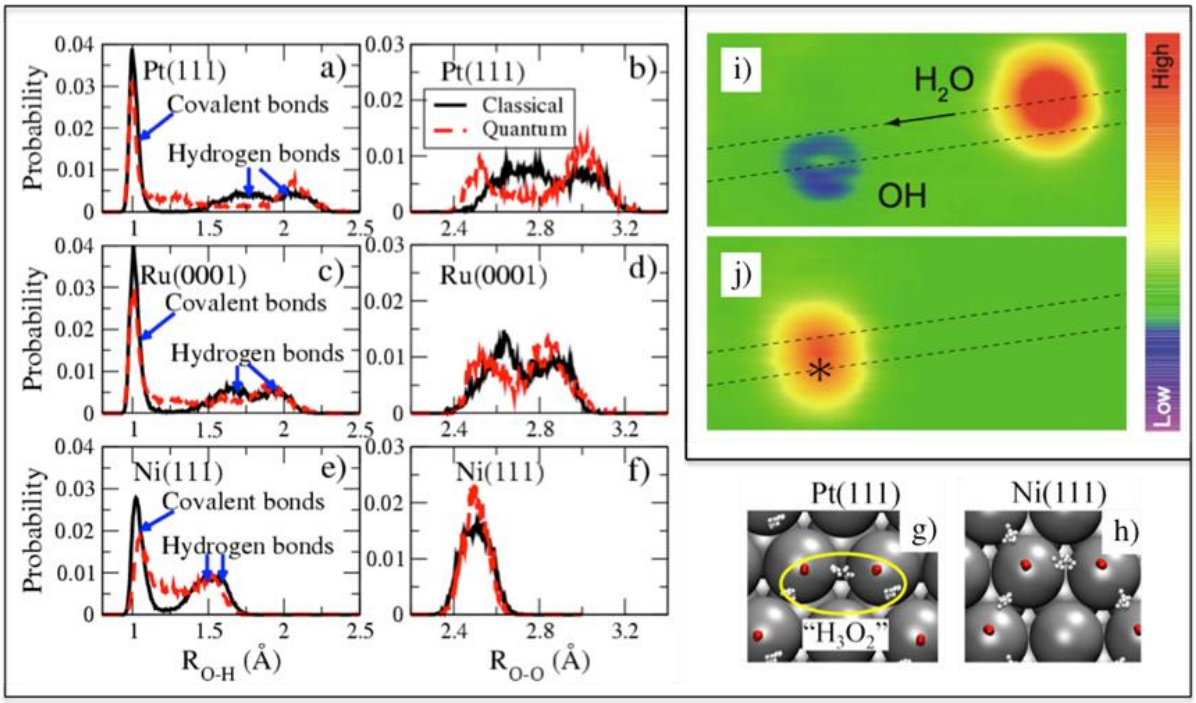

Figure 6. Evidence for strong quantum effects for water adsorbed on metal surfaces. Left: Simulation results for selected structural properties of extended water-hydroxyl overlayers on metal surfaces. Probability distributions of O-H [(a), (c), (e)] and O-O distances [(b), (d), (f)] on Pt, Ru, and Ni at 160 K, as obtained from MD with classical nuclei (labeled classical, black solid lines) and PIMD [labeled quantum, (red) dashed lines]. On the bottom right snapshots for typical spatial configurations of the overlayer on Pt (g), and Ni (h) obtained from PIMD (with every atom represented by 16 beads) are shown. On Pt and Ru at any given snapshot one proton is equally shared by two of the O's yielding an intermediate HO-H-OH-like complex. On Ni at any given snapshot several protons can simultaneously be shared between the oxygens. Panels (a)-(h) are adapted from Ref. (91) (Copyright 2010 American Physical Society). Upper right: Scanning tunneling microscopy images before (i) and after (j) the formation of a water-hydroxyl dimer on Cu(110). Reprinted with permission from Ref. (92) (Copyright 2010 American Physical

Society). The symmetric nature of the dimer in j implies that the hydrogen between the two oxygens in this structure is shared symmetrically. Figure created from.

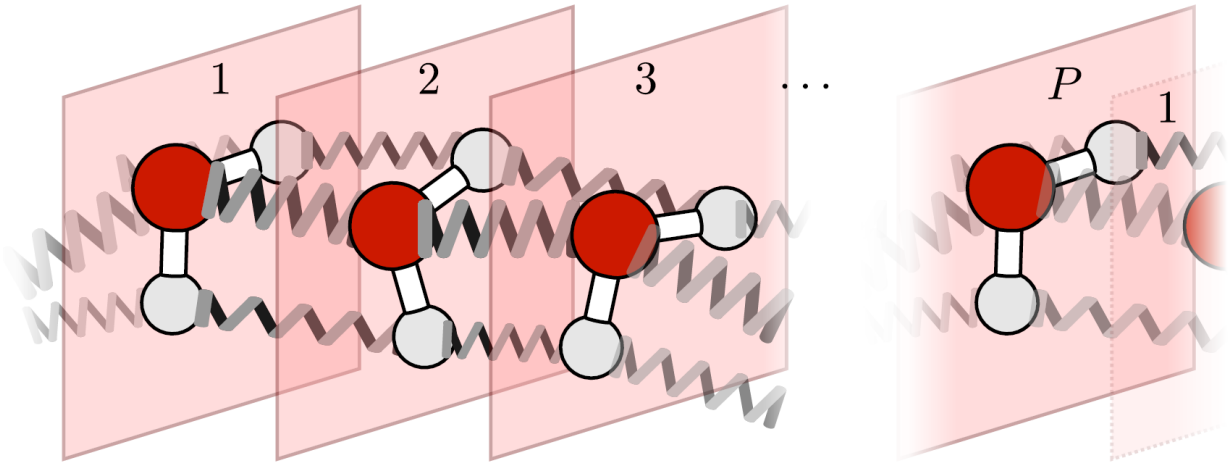

Figure 7. Representation of the imaginary time path integral isomorphism exploited in PIMD, RPMD and CMD. Each replica (bead) of the system is connected by harmonic springs to its adjacent replica. Note that due to the cyclic boundary conditions the P^{th} (last) ring polymer replica is connected to the first one.

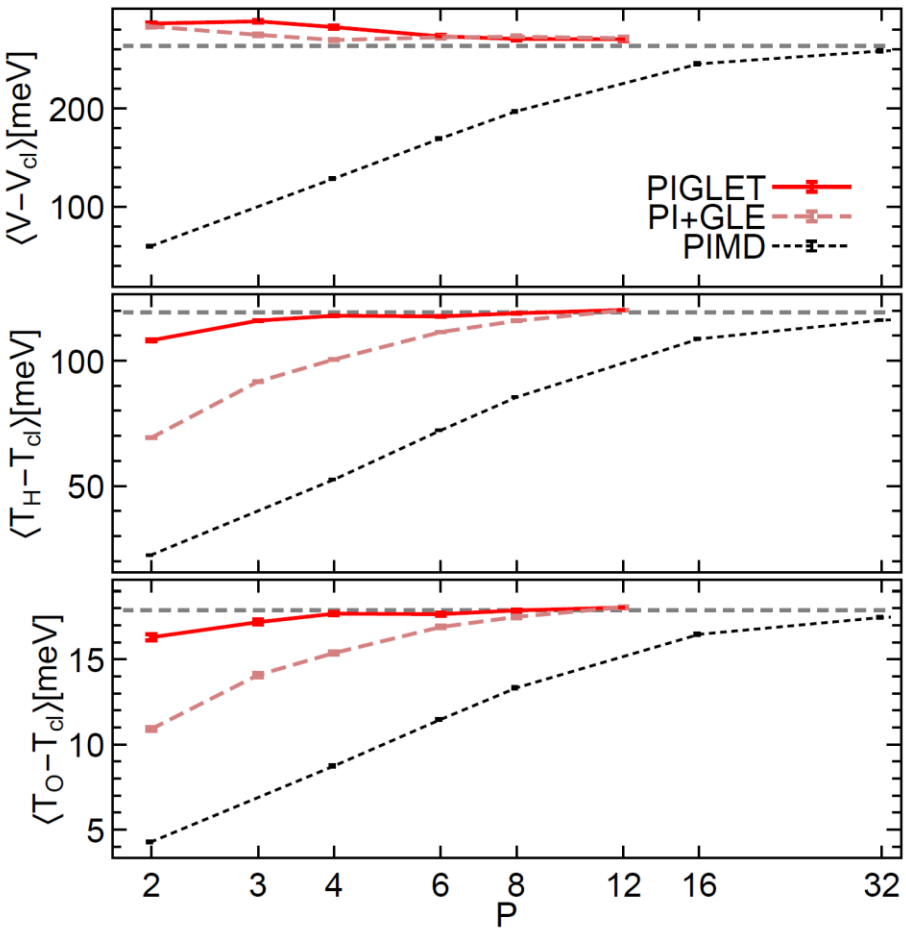

Figure 8. The quantum contribution to the potential energy, and to the kinetic energy of hydrogen and oxygen atoms as computed by the centroid virial estimator for a simulation of a flexible water model(4) at T=298 K, plotted as a function of the number of beads. Note the much accelerated convergence rate of the kinetic energy when using PIGLET compared to PI+GLE. (Adapted from Ref. (14))

Biographies

Michele Ceriotti received his Ph.D. in Physics from ETH Zürich, under the supervision of Prof. Michele Parrinello. He was then awarded a Swiss National Science foundation post-graduate fellowship, as well as a Royal Society Newton International Fellowship and a Marie Curie Intra-European Fellowship, with which he spent three years in Oxford in the Physical and Theoretical Chemistry Laboratory, working with Prof. David E. Manolopoulos. During his time in Oxford,

he was also appointed as a Junior Research Fellow at Merton College. Since November 2013 he works as an assistant professor at the Institute of Materials at EPFL Lausanne, where he leads the laboratory for Computational Science and Modeling. His research interests focus on the development of methods for molecular dynamics and the simulation of complex systems at the atomistic level, and to their application to problems in chemistry and materials science. He developed accelerated techniques to model nuclear quantum effects based on a generalized Langevin equation, and applies them to the study of water and hydrogen-bonded systems.

Wei Fang is a Ph.D. student in Prof. Angelos Michaelides' group at University College London. He received his bachelor degree in Physics at Peking University in 2013. His Ph.D. project focuses on studying nuclear quantum effects in hydrogen-bonded systems.

Peter G. Kusalik earned his M.Sc. and Ph.D. degrees in Chemistry at the University of British Columbia. After completing a postdoctoral fellowship at the Australian National University, he moved to the Department of Chemistry at Dalhousie University. While at Dalhousie he received tenure and was promoted to the rank of Professor. In 2005 he moved to the University of Calgary, where he has served as Head of the Department of Chemistry and as Associate Dean in the Faculty of Science. His research interests center on utilizing molecular simulations to provide insights into the behavior in liquids, solutions and solids at the microscopic level. Aqueous systems have been a primary focus of much of his research, where explorations of crystal nucleation and growth have been a focal point for much of his group's recent work.

Ross McKenzie is a Professor of Physics at The University of Queensland in Brisbane, Australia. He was an undergraduate at the Australian National University and received a PhD from Princeton University in 1989. Ross' research involves using quantum many-body theory to understand the properties of complex materials, ranging from fluorescent proteins to molecular superconductors. He is author of the blog, Condensed Concepts: Ruminations on emergent phenomena in condensed phases of matter [condensedconcepts.blogspot.com]. Co-authorship of this review continues a family tradition. In 1978 and 1983, Ross' father, Hugh A. McKenzie, together with John T. Edsall, wrote reviews about water and its interaction with electrolytes and proteins.

Angelos Michaelides obtained a Ph.D. in Theoretical Chemistry in 2000 from The Queen's University of Belfast. Following this he worked as a post-doctoral research associate and junior research fellow at the University of Cambridge and then at the Fritz Haber Institute, Berlin, as an Alexander von Humboldt research fellow. Subsequently he was promoted to staff scientist and research group leader at the Fritz Haber Institute. In 2006 he moved to University College London, where since 2009 he has been Professor of Theoretical Chemistry. Research in his group (www.chem.ucl.ac.uk/ice) involves computer simulations of catalytic and environmental interfaces, aiming at reaching fundamental new understanding of elementary processes at such interfaces. Water is a major focus of their work.

Miguel A. Morales received his Ph.D. in Physics from the University of Illinois at Urbana-Champaign under the supervision of Prof. David M. Ceperley. After postdoctoral work at Rice University in the group of Prof. Gustavo E. Scuseria, he moved to Lawrence Livermore National Laboratory where he currently works as a Research Scientist. His research focuses on the study of light materials at extreme conditions, with a particular emphasis on nuclear quantum effects and their influence on thermodynamic and structural properties. He also works on the development of predictive quantum simulation methods based on quantum Monte Carlo approaches.

Thomas E. Markland received his D.Phil. in Chemistry from Balliol College, University of Oxford in 2009 under the supervision of Prof. David E. Manolopoulos. After postdoctoral work with Prof. Bruce J. Berne at Columbia University he moved to Stanford University in 2011 as an Assistant Professor in the Department of Chemistry. His research interests lie broadly in the development of theoretical and simulation methods and their application to explain effects observed in the classical and quantum dynamics of chemical systems. He has introduced numerous algorithms to improve the efficiency of quantum path integral approaches and was an early developer of the ring polymer molecular dynamics method. He has applied these developments to elucidate the role of quantum mechanics in hydrogen bonded systems ranging from water to enzymatic proton networks.

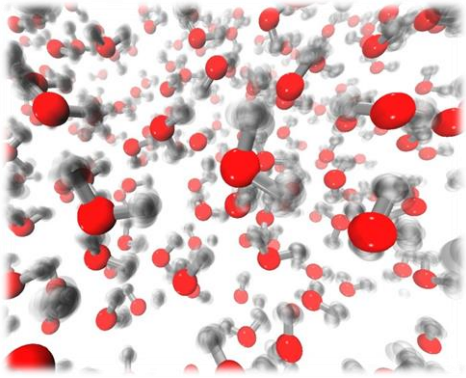

TOC Image

References

1. Anonymous (!!! INVALID CITATION !!! (1-3)).
2. McKenzie RH, Bekker C, Athokpam B, & Ramesh SG (2014) Effect of quantum nuclear motion on hydrogen bonding. *J Chem Phys* 140(17).
3. McKenzie RH (2012) A diabatic state model for donor-hydrogen vibrational frequency shifts in hydrogen bonded complexes. *Chem Phys Lett* 535:196-200.

4. Habershon S, Markland TE, & Manolopoulos DE (2009) Competing quantum effects in the dynamics of a flexible water model. *J Chem Phys* 131(2).
5. Chen B, Ivanov I, Klein ML, & Parrinello M (2003) Hydrogen bonding in water. *Phys Rev Lett* 91(21).
6. Markland TE & Berne BJ (2012) Unraveling quantum mechanical effects in water using isotopic fractionation. *P Natl Acad Sci USA* 109(21):7988-7991.
7. Li XZ, Walker B, & Michaelides A (2011) Quantum nature of the hydrogen bond. *P Natl Acad Sci USA* 108(16):6369-6373.
8. Ceriotti M & Markland TE (2013) Efficient methods and practical guidelines for simulating isotope effects. *J Chem Phys* 138(1).
9. Habershon S, Manolopoulos DE, Markland TE, & Miller TF (2013) Ring-Polymer Molecular Dynamics: Quantum Effects in Chemical Dynamics from Classical Trajectories in an Extended Phase Space. *Annu Rev Phys Chem* 64:387-413.
10. Ceriotti M, Parrinello M, Markland TE, & Manolopoulos DE (2010) Efficient stochastic thermostatting of path integral molecular dynamics. *J Chem Phys* 133(12).
11. Fanourgakis GS, Markland TE, & Manolopoulos DE (2009) A fast path integral method for polarizable force fields. *J Chem Phys* 131(9).
12. Markland TE & Manolopoulos DE (2008) A refined ring polymer contraction scheme for systems with electrostatic interactions. *Chem Phys Lett* 464(4-6):256-261.
13. Markland TE & Manolopoulos DE (2008) An efficient ring polymer contraction scheme for imaginary time path integral simulations. *J Chem Phys* 129(2).
14. Ceriotti M & Manolopoulos DE (2012) Efficient First-Principles Calculation of the Quantum Kinetic Energy and Momentum Distribution of Nuclei. *Phys Rev Lett* 109(10).
15. Ceriotti M, Manolopoulos DE, & Parrinello M (2011) Accelerating the convergence of path integral dynamics with a generalized Langevin equation. *J Chem Phys* 134(8).
16. Perez A & Tuckerman ME (2011) Improving the convergence of closed and open path integral molecular dynamics via higher order Trotter factorization schemes. *J Chem Phys* 135(6).
17. Morrone JA & Car R (2008) Nuclear quantum effects in water. *Phys Rev Lett* 101(1).
18. Wang L, Ceriotti M, & Markland TE (2014) Quantum fluctuations and isotope effects in ab initio descriptions of water. *J Chem Phys* 141(10).
19. Ceriotti M, Cuny J, Parrinello M, & Manolopoulos DE (2013) Nuclear quantum effects and hydrogen bond fluctuations in water. *P Natl Acad Sci USA* 110(39):15591-15596.
20. Marx D & Parrinello M (1994) Ab-Initio Path-Integral Molecular-Dynamics. *Z Phys B Con Mat* 95(2):143-144.
21. Tuckerman ME, Marx D, Klein ML, & Parrinello M (1996) Efficient and general algorithms for path integral Car-Parrinello molecular dynamics. *J Chem Phys* 104(14):5579-5588.
22. Marx D & Parrinello M (1996) Ab initio path integral molecular dynamics: Basic ideas. *J Chem Phys* 104(11):4077-4082.
23. Wang YM, Huang XC, Shepler BC, Braams BJ, & Bowman JM (2011) Flexible, ab initio potential, and dipole moment surfaces for water. I. Tests and applications for clusters up to the 22-mer. *J Chem Phys* 134(9).
24. Fanourgakis GS & Xantheas SS (2008) Development of transferable interaction potentials for water. V. Extension of the flexible, polarizable, Thole-type model potential

(TTM3-F, v. 3.0) to describe the vibrational spectra of water clusters and liquid water. *J Chem Phys* 128(7).
25. Burnham CJ & Xantheas SS (2002) Development of transferable interaction models for water. IV. A flexible, all-atom polarizable potential (TTM2-F) based on geometry dependent charges derived from an ab initio monomer dipole moment surface. *J Chem Phys* 116(12):5115-5124.
26. Burnham CJ, Anick DJ, Mankoo PK, & Reiter GF (2008) The vibrational proton potential in bulk liquid water and ice. *J Chem Phys* 128(15).
27. Medders GR, Babin V, & Paesani F (2014) Development of a "First-Principles" Water Potential with Flexible Monomers. III. Liquid Phase Properties. *J Chem Theory Comput* 10(8):2906-2910.
28. Senesi R, Romanelli G, Adams MA, & Andreani C (2013) Temperature dependence of the zero point kinetic energy in ice and water above room temperature. *Chem Phys* 427:111-116.
29. Andreani C, Romanelli G, & Senesi R (2013) A combined INS and DINS study of proton quantum dynamics of ice and water across the triple point and in the supercritical phase. *Chem Phys* 427:106-110.
30. Romanelli G, *et al.* (2013) Direct Measurement of Competing Quantum Effects on the Kinetic Energy of Heavy Water upon Melting. *J Phys Chem Lett* 4(19):3251-3256.
31. Senesi R, *et al.* (2013) The quantum nature of the OH stretching mode in ice and water probed by neutron scattering experiments. *J Chem Phys* 139(7).
32. Andreani C, Colognesi D, Pietropaolo A, & Senesi R (2011) Ground state proton dynamics in stable phases of water. *Chem Phys Lett* 518:1-6.
33. Pietropaolo A, Senesi R, Andreani C, & Mayers J (2009) Quantum Effects in Water: Proton Kinetic Energy Maxima in Stable and Supercooled Liquid. *Braz J Phys* 39(2):318-321.
34. Pantalei C, *et al.* (2008) Proton momentum distribution of liquid water from room temperature to the supercritical phase. *Phys Rev Lett* 100(17).
35. Pietropaolo A, *et al.* (2008) Excess of proton mean kinetic energy in supercooled water. *Phys Rev Lett* 100(12).
36. Botti A, *et al.* (2007) Structure and single proton dynamics of bulk supercooled water. *J Mol Liq* 136(3):236-240.
37. Garbuio V, *et al.* (2007) Proton quantum coherence observed in water confined in silica nanopores. *J Chem Phys* 127(15).
38. Andreani C, Colognesi D, Degiorgi E, & Ricci MA (2001) Proton dynamics in supercritical water. *J Chem Phys* 115(24):11243-11248.
39. Reiter GF, *et al.* (2013) Anomalous Ground State of the Electrons in Nanoconfined Water. *Phys Rev Lett* 111(3).
40. Reiter GF, *et al.* (2012) Evidence for an anomalous quantum state of protons in nanoconfined water. *Phys Rev B* 85(4).
41. Burnham CJ, *et al.* (2011) The proton momentum distribution in strongly H-bonded phases of water: A critical test of electrostatic models. *J Chem Phys* 135(14).
42. Reiter GF, Li JC, Mayers J, Platzman P, & Stillinger F (2004) The proton momentum distribution in water and ice. *Braz J Phys* 34(1):142-147.
43. Mosin OV, Shvets VI, Skladnev DA, & Ignatov I (2012) STUDYING OF MICROBIC SYNTHESIS OF DEUTERIUM LABELLED L-PHENYLALANINE BY

METHYLOTROPHIC BACTERIUM Brevibacterium methylicum ON MEDIA WITH DIFFERENY CONTENT OF HEAVY WATER. *Russian Journal of Biopharmaceuticals* 4(1).
44. Kushner DJ, Baker A, & Dunstall TG (1999) Pharmacological uses and perspectives of heavy water and deuterated compounds. *Can J Physiol Pharm* 77(2):79-88.
45. Thomson JF (1960) PHYSIOLOGICAL EFFECTS OF D2O IN MAMMALS*. *Annals of the New York Academy of Sciences* 84(16):736-744.
46. Czajka DM, Fischer CS, Finkel AJ, & Katz JJ (1961) Physiological Effects of Deuterium on Dogs. *Am J Physiol* 201(2):357-&.
47. Lin L, Morrone JA, & Car R (2011) Correlated Tunneling in Hydrogen Bonds. *J Stat Phys* 145(2):365-384.
48. Schweizer KS & Stillinger FH (1984) Phase-Transitions Induced by Proton Tunneling in Hydrogen-Bonded Crystals - Ground-State Theory. *Phys Rev B* 29(1):350-360.
49. Schweizer KS & Stillinger FH (1984) High-Pressure Phase-Transitions and Hydrogen-Bond Symmetry in Ice Polymorphs. *J Chem Phys* 80(3):1230-1240.
50. Stillinger FH & Schweizer KS (1983) Ice under Pressure - Transition to Symmetrical Hydrogen-Bonds. *J Phys Chem-Us* 87(21):4281-4288.
51. Benoit M, Marx D, & Parrinello M (1998) Tunnelling and zero-point motion in high-pressure ice. *Nature* 392(6673):258-261.
52. Yen F & Gao T (2015) Dielectric Anomaly in Ice near 20 K: Evidence of Macroscopic Quantum Phenomena. *J Phys Chem Lett* 6(14):2822-2825.
53. Drechsel-Grau C & Marx D (2014) Exceptional Isotopic-Substitution Effect: Breakdown of Collective Proton Tunneling in Hexagonal Ice due to Partial Deuteration. *Angew Chem Int Edit* 53(41):10937-10940.
54. Drechsel-Grau C & Marx D (2014) Quantum Simulation of Collective Proton Tunneling in Hexagonal Ice Crystals. *Phys Rev Lett* 112(14).
55. Wang L, Fried SD, Boxer SG, & Markland TE (2014) Quantum delocalization of protons in the hydrogen-bond network of an enzyme active site. *P Natl Acad Sci USA* 111(52):18454-18459.
56. Zachos J, Pagani M, Sloan L, Thomas E, & Billups K (2001) Trends, rhythms, and aberrations in global climate 65 Ma to present. *Science* 292(5517):686-693.
57. Worden J, Noone D, Bowman K, & Spect TE (2007) Importance of rain evaporation and continental convection in the tropical water cycle. *Nature* 445(7127):528-532.
58. Csaszar AG, *et al.* (2005) On equilibrium structures of the water molecule. *J Chem Phys* 122(21).
59. Wang YM, Babin V, Bowman JM, & Paesani F (2012) The Water Hexamer: Cage, Prism, or Both. Full Dimensional Quantum Simulations Say Both. *J Am Chem Soc* 134(27):11116-11119.
60. Babin V & Paesani F (2013) The curious case of the water hexamer: Cage vs. Prism. *Chem Phys Lett* 580:1-8.
61. Liu K, *et al.* (1996) Characterization of a cage form of the water hexamer. *Nature* 381(6582):501-503.
62. Habershon S & Manolopoulos DE (2011) Free energy calculations for a flexible water model. *Phys Chem Chem Phys* 13(44):19714-19727.
63. McBride C, Aragones JL, Noya EG, & Vega C (2012) A study of the influence of isotopic substitution on the melting point and temperature of maximum density of water

by means of path integral simulations of rigid models. *Phys Chem Chem Phys* 14(43):15199-15205.
64. Ramirez R & Herrero CP (2010) Quantum path integral simulation of isotope effects in the melting temperature of ice Ih. *J Chem Phys* 133(14).
65. McBride C, Noya EG, Aragones JL, Conde MM, & Vega C (2012) The phase diagram of water from quantum simulations. *Phys Chem Chem Phys* 14(29):10140-10146.
66. Vega C, *et al.* (2010) Heat capacity of water: A signature of nuclear quantum effects. *J Chem Phys* 132(4).
67. Schmidt J, *et al.* (2009) Isobaric-Isothermal Molecular Dynamics Simulations Utilizing Density Functional Theory: An Assessment of the Structure and Density of Water at Near-Ambient Conditions. *J Phys Chem B* 113(35):11959-11964.
68. Anonymous (IAPWS, http://www.iapws.org/release.html (accessed 21 Dec. 2014).
69. Anonymous (1999) CRC handbook of chemistry and physics. (Chapman and Hall/CRCnetBASE,, Boca Raton, FL), pp CD-ROMs.
70. Pamuk B, *et al.* (2012) Anomalous Nuclear Quantum Effects in Ice. *Phys Rev Lett* 108(19).
71. Bergmann U, *et al.* (2007) Isotope effects in liquid water probed by x-ray Raman spectroscopy. *Phys Rev B* 76(2).
72. Harada Y, *et al.* (2013) Selective Probing of the OH or OD Stretch Vibration in Liquid Water Using Resonant Inelastic Soft-X-Ray Scattering. *Phys Rev Lett* 111(19).
73. Nilsson A, *et al.* (2010) X-ray absorption spectroscopy and X-ray Raman scattering of water and ice; an experimental view. *Journal of Electron Spectroscopy and Related Phenomena* 177(2-3):99-129.
74. Nilsson A & Pettersson LGM (2011) Perspective on the structure of liquid water. *Chem Phys* 389(1-3):1-34.
75. Wernet P, *et al.* (2004) The structure of the first coordination shell in liquid water. *Science* 304(5673):995-999.
76. Huang C, *et al.* (2009) The inhomogeneous structure of water at ambient conditions. *P Natl Acad Sci USA* 106(36):15214-15218.
77. Tokushima T, *et al.* (2010) High resolution X-ray emission spectroscopy of water and its assignment based on two structural motifs. *Journal of Electron Spectroscopy and Related Phenomena* 177(2-3):192-205.
78. Tokushima T, *et al.* (2008) High resolution X-ray emission spectroscopy of liquid water: The observation of two structural motifs. *Chem Phys Lett* 460(4-6):387-400.
79. Root JH, Egelstaff PA, & Hime A (1986) QUANTUM EFFECTS IN THE STRUCTURE OF WATER MEASURED BY GAMMA-RAY DIFFRACTION. *Chem Phys* 109(2-3):437-453.
80. Soper AK & Benmore CJ (2008) Quantum differences between heavy and light water. *Phys Rev Lett* 101(6).
81. Tomberli B, Benmore CJ, Egelstaff PA, Neuefeind J, & Honkimaki V (2000) Isotopic quantum effects in water structure measured with high energy photon diffraction. *J Phys-Condens Mat* 12(12):2597-2612.
82. Zeidler A, *et al.* (2012) Zeidler et al. Reply. *Phys Rev Lett* 108(25).
83. Zeidler A, *et al.* (2012) Isotope effects in water as investigated by neutron diffraction and path integral molecular dynamics. *J Phys-Condens Mat* 24(28).

84. Zeidler A, *et al.* (2011) Oxygen as a Site Specific Probe of the Structure of Water and Oxide Materials. *Phys Rev Lett* 107(14).
85. Yoshida K, Matubayasi N, & Nakahara M (2008) Self-diffusion coefficients for water and organic solvents at high temperatures along the coexistence curve. *J Chem Phys* 129(21).
86. Hirsch KR & Holzapfel WB (1986) Effect of High-Pressure on the Raman-Spectra of Ice-Viii and Evidence for Ice-X. *J Chem Phys* 84(5):2771-2775.
87. Hirsch KR & Holzapfel WB (1984) Symmetric Hydrogen-Bonds in Ice-X. *Phys Lett A* 101(3):142-144.
88. Ogasawara H, *et al.* (2002) Structure and bonding of water on Pt(111). *Phys Rev Lett* 89(27).
89. Carrasco J, Hodgson A, & Michaelides A (2012) A molecular perspective of water at metal interfaces. *Nat Mater* 11(8):667-674.
90. Hodgson A & Haq S (2009) Water adsorption and the wetting of metal surfaces. *Surf Sci Rep* 64(9):381-451.
91. Li XZ, Probert MIJ, Alavi A, & Michaelides A (2010) Quantum Nature of the Proton in Water-Hydroxyl Overlayers on Metal Surfaces. *Phys Rev Lett* 104(6).
92. Kumagai T, *et al.* (2010) Symmetric hydrogen bond in a water-hydroxyl complex on Cu(110). *Phys Rev B* 81(4).
93. Meng XZ, *et al.* (2015) Direct visualization of concerted proton tunnelling in a water nanocluster. *Nat Phys* 11(3):235-239.
94. Kresheck GC, Schneide.H, & Scheraga HA (1965) Effect of D20 on Thermal Stability of Proteins . Thermodynamic Parameters for Transfer of Model Compounds from H2o to D2o. *J Phys Chem-Us* 69(9):3132-&.
95. Hermans J & Scheraga HA (1959) The Thermally Induced Configurational Change of Ribonuclease in H2o and D2o. *Biochim Biophys Acta* 36(2):534-535.
96. Shirota H, Pal H, Tominaga K, & Yoshihara K (1996) Deuterium isotope effect on the solvation dynamics of methanol: CH3OH, CH3OD, CD3OH, and CD3OD. *J Phys Chem-Us* 100(35):14575-14577.
97. Lopez MM & Makhatadze GI (1998) Solvent isotope effect on thermodynamics of hydration. *Biophys Chem* 74(2):117-125.
98. Graziano G (2000) On the solvent isotope effect in hydrophobic hydration. *J Phys Chem B* 104(39):9249-9254.
99. Diken EG, Shin JW, Price EA, & Johnson MA (2004) Isotopic fractionation and zero-point effects in anionic H-bonded complexes: a comparison of the I-center dot HDO and F-center dot HDO ion-molecule clusters. *Chem Phys Lett* 387(1-3):17-22.
100. Wilkins DM, Manolopoulos DE, & Dang LX (2015) Nuclear quantum effects in water exchange around lithium and fluoride ions. *J Chem Phys* 142(6).
101. Habershon S (2014) Zero-point energy effects in anion solvation shells. *Phys Chem Chem Phys* 16(19):9154-9160.
102. Schmitt UW & Voth GA (2000) The isotope substitution effect on the hydrated proton. *Chem Phys Lett* 329(1-2):36-41.
103. Pavese M, Chawla S, Lu DS, Lobaugh J, & Voth GA (1997) Quantum effects and the excess proton in water. *J Chem Phys* 107(18):7428-7432.
104. Lobaugh J & Voth GA (1996) The quantum dynamics of an excess proton in water. *J Chem Phys* 104(5):2056-2069.

105. Wong KF, *et al.* (2010) Proton Transfer Studied Using a Combined Ab Initio Reactive Potential Energy Surface with Quantum Path Integral Methodology. *J Chem Theory Comput* 6(9):2566-2580.
106. Marx D, Tuckerman ME, & Parrinello M (2000) Solvated excess protons in water: quantum effects on the hydration structure. *J Phys-Condens Mat* 12(8a):A153-A159.
107. Marx D (2006) Proton transfer 200 years after von Grotthuss: Insights from ab initio simulations. *Chemphyschem* 7(9):1848-1870.
108. Tuckerman ME, Marx D, & Parrinello M (2002) The nature and transport mechanism of hydrated hydroxide ions in aqueous solution. *Nature* 417(6892):925-929.
109. Hassanali A, Prakash MK, Eshet H, & Parrinello M (2011) On the recombination of hydronium and hydroxide ions in water. *P Natl Acad Sci USA* 108(51):20410-20415.
110. Markland TE, Habershon S, & Manolopoulos DE (2008) Quantum diffusion of hydrogen and muonium atoms in liquid water and hexagonal ice. *J Chem Phys* 128(19).
111. Deraedt B, Sprik M, & Klein ML (1984) Computer-Simulation of Muonium in Water. *J Chem Phys* 80(11):5719-5724.
112. Yoshikawa T & Takayanagi T (2014) Nonadiabatic Relaxation Dynamics of Water Anion Cluster and Its Isotope Effects by Ring-Polymer Molecular Dynamics Simulation. *Int J Quantum Chem* 114(10):636-641.
113. Yoshikawa T & Takayanagi T (2013) Application of ring-polymer molecular dynamics to electronically nonadiabatic excess electron dynamics in water clusters: Importance of nuclear quantum effects. *Chem Phys Lett* 564:1-5.
114. Marsalek O, Uhlig F, Vandevondele J, & Jungwirth P (2012) Structure, Dynamics, and Reactivity of Hydrated Electrons by Ab Initio Molecular Dynamics. *Accounts Chem Res* 45(1):23-32.
115. Marsalek O, *et al.* (2010) Hydrogen Forms in Water by Proton Transfer to a Distorted Electron. *J Phys Chem B* 114(2):915-920.
116. Turi L, Sheu WS, & Rossky PJ (2005) Characterization of excess electrons in water-cluster anions by quantum simulations. *Science* 309(5736):914-917.
117. Jacobson LD & Herbert JM (2011) Theoretical Characterization of Four Distinct Isomer Types in Hydrated-Electron Clusters, and Proposed Assignments for Photoelectron Spectra of Water Cluster Anions. *J Am Chem Soc* 133(49):19889-19899.
118. Ma L, Majer K, Chirot F, & von Issendorff B (2009) Low temperature photoelectron spectra of water cluster anions. *J Chem Phys* 131(14).
119. Turi L (2015) Hydrated Electrons in Water Clusters: Inside or Outside, Cavity or Noncavity? *J Chem Theory Comput* 11(4):1745-1755.
120. Larsen RE, Glover WJ, & Schwartz BJ (2010) Does the Hydrated Electron Occupy a Cavity? *Science* 329(5987):65-69.
121. Tuckerman ME, Marx D, Klein ML, & Parrinello M (1997) On the quantum nature of the shared proton in hydrogen bonds. *Science* 275(5301):817-820.
122. Chen J, Li XZ, Zhang QF, Michaelides A, & Wang EG (2013) Nature of proton transport in a water-filled carbon nanotube and in liquid water. *Phys Chem Chem Phys* 15(17):6344-6349.
123. Roberts NK & Northey HL (1974) Proton and Deuteron Mobility in Normal and Heavy-Water Solutions of Electrolytes. *J Chem Soc Farad T 1* 70(2):253-262.
124. Bartels DM, Han P, & Percival PW (1993) Diffusion of Atomic-Hydrogen in Ice-Ih. *Chem Phys Lett* 210(1-3):129-134.

125. Bartels DM, Han P, & Percival PW (1992) Diffusion and Cidep of H and D Atoms in Solid H2o, D2o and Isotopic Mixtures. *Chem Phys* 164(3):421-437.
126. Benderskii VA & Krivenko AG (1996) Diffusion of hydrogen and deuterium atoms in water. *Russ J Electrochem*+ 32(6):663-669.
127. Petit JR, *et al.* (1999) Climate and atmospheric history of the past 420,000 years from the Vostok ice core, Antarctica. *Nature* 399(6735):429-436.
128. Vanicek J & Miller WH (2007) Efficient estimators for quantum instanton evaluation of the kinetic isotope effects: Application to the intramolecular hydrogen transfer in pentadiene. *J Chem Phys* 127(11).
129. Vanicek J, Miller WH, Castillo JF, & Aoiz FJ (2005) Quantum-instanton evaluation of the kinetic isotope effects. *J Chem Phys* 123(5).
130. Andreani C, Colognesi D, Mayers J, Reiter GF, & Senesi R (2005) Measurement of momentum distribution of light atoms and molecules in condensed matter systems using inelastic neutron scattering. *Adv Phys* 54(5):377-469.
131. Lin L, Morrone JA, Car R, & Parrinello M (2011) Momentum distribution, vibrational dynamics, and the potential of mean force in ice. *Phys Rev B* 83(22).
132. Lin L, Morrone JA, Car R, & Parrinello M (2010) Displaced Path Integral Formulation for the Momentum Distribution of Quantum Particles. *Phys Rev Lett* 105(11).
133. Morrone JA, Lin L, & Car R (2009) Tunneling and delocalization effects in hydrogen bonded systems: A study in position and momentum space. *J Chem Phys* 130(20).
134. Morrone JA, Srinivasan V, Sebastiani D, & Car R (2007) Proton momentum distribution in water: an open path integral molecular dynamics study. *J Chem Phys* 126(23).
135. Paesani F, Zhang W, Case DA, Cheatham TE, & Voth GA (2006) An accurate and simple quantum model for liquid water. *J Chem Phys* 125(18).
136. Wallqvist A & Berne BJ (1985) Path-Integral Simulation of Pure Water. *Chem Phys Lett* 117(3):214-219.
137. Kuharski RA & Rossky PJ (1985) A Quantum-Mechanical Study of Structure in Liquid H2o and D2o. *J Chem Phys* 82(11):5164-5177.
138. de la Pena LH & Kusalik PG (2006) Quantum effects in liquid water and ice: Model dependence. *J Chem Phys* 125(5).
139. Marsalek O & Markland TE (2016) Ab initio molecular dynamics with nuclear quantum effects at classical cost: Ring polymer contraction for density functional theory. *The Journal of Chemical Physics* 144(5):054112.
140. Marzari N & Vanderbilt D (1997) Maximally localized generalized Wannier functions for composite energy bands. *Phys Rev B* 56(20):12847-12865.
141. Sun JM, Clark BK, Torquato S, & Car R (2015) The phase diagram of high-pressure superionic ice. *Nat Commun* 6.
142. Liu J, *et al.* (2013) A Surface-Specific Isotope Effect in Mixtures of Light and Heavy Water. *J Phys Chem C* 117(6):2944-2951.
143. Zimmermann T & Vanicek J (2009) Path integral evaluation of equilibrium isotope effects. *J Chem Phys* 131(2).
144. Marsalek O, *et al.* (2014) Efficient Calculation of Free Energy Differences Associated with Isotopic Substitution Using Path-Integral Molecular Dynamics. *J Chem Theory Comput* 10(4):1440-1453.
145. Morales MA, *et al.* (2014) Quantum Monte Carlo Benchmark of Exchange-Correlation Functionals for Bulk Water. *J Chem Theory Comput* 10(6):2355-2362.

146. Zhang C, Wu J, Galli G, & Gygi F (2011) Structural and Vibrational Properties of Liquid Water from van der Waals Density Functionals. *J Chem Theory Comput* 7(10):3054-3061.
147. Santra B, Michaelides A, & Scheffler M (2009) Coupled cluster benchmarks of water monomers and dimers extracted from density-functional theory liquid water: The importance of monomer deformations. *J Chem Phys* 131(12).
148. Gillan MJ, Alfe D, Bartok AP, & Csanyi G (2013) First-principles energetics of water clusters and ice: A many-body analysis. *J Chem Phys* 139(24).
149. Mei HS, Tuckerman ME, Sagnella DE, & Klein ML (1998) Quantum nuclear ab initio molecular dynamics study of water wires. *J Phys Chem B* 102(50):10446-10458.
150. Ranea VA, *et al.* (2004) Water dimer diffusion on Pd{111} assisted by an H-bond donor-acceptor tunneling exchange. *Phys Rev Lett* 92(13).
151. Voth GA (2006) Computer simulation of proton solvation and transport in aqueous and biomolecular systems. *Accounts Chem Res* 39(2):143-150.
152. Kumagai T, *et al.* (2008) Direct observation of hydrogen-bond exchange within a single water dimer. *Phys Rev Lett* 100(16).
153. Alfe D & Gillan MJ (2010) Ab initio statistical mechanics of surface adsorption and desorption. II. Nuclear quantum effects. *J Chem Phys* 133(4).
154. Cao Z, *et al.* (2010) Mechanism of Fast Proton Transport along One-Dimensional Water Chains Confined in Carbon Nanotubes. *J Am Chem Soc* 132(33):11395-11397.
155. Michaelides A, Ranea VA, de Andres PL, & King DA (2003) General model for water monomer adsorption on close-packed transition and noble metal surfaces. *Phys Rev Lett* 90(21).
156. Kumagai T (2015) Direct observation and control of hydrogen-bond dynamics using low-temperature scanning tunneling microscopy. *Prog Surf Sci* 90(3):239-291.
157. Aqvist J & Warshel A (1993) Simulation of Enzyme-Reactions Using Valence-Bond Force-Fields and Other Hybrid Quantum-Classical Approaches. *Chem Rev* 93(7):2523-2544.
158. Schmitt UW & Voth GA (1998) Multistate empirical valence bond model for proton transport in water. *J Phys Chem B* 102(29):5547-5551.
159. Vuilleumier R & Borgis D (1998) Quantum dynamics of an excess proton in water using an extended empirical valence-bond Hamiltonian. *J Phys Chem B* 102(22):4261-4264.
160. Vuilleumier R & Borgis D (1998) An extended empirical valence bond model for describing proton transfer in H+(H2O)(n) clusters and liquid water. *Chem Phys Lett* 284(1-2):71-77.
161. Warshel A & Weiss RM (1980) An Empirical Valence Bond Approach for Comparing Reactions in Solutions and in Enzymes. *J Am Chem Soc* 102(20):6218-6226.
162. Tennyson J, *et al.* (2014) IUPAC critical evaluation of the rotational-vibrational spectra of water vapor. Part IV. Energy levels and transition wavenumbers for (D2O)-O-16, (D2O)-O-17, and (D2O)-O-18. *J Quant Spectrosc Ra* 142:93-108.
163. Anonymous (National Insitute of Standards and Technology (NIST) Chemistry WebBooks. Availiable at http://webbook.nist.gov (accesssed 19 Dec. 2014).
164. Yoshimura Y, Stewart ST, Somayazulu M, Mao H, & Hemley RJ (2006) High-pressure x-ray diffraction and Raman spectroscopy of ice VIII. *J Chem Phys* 124(2).
165. Murray ED & Galli G (2012) Dispersion Interactions and Vibrational Effects in Ice as a Function of Pressure: A First Principles Study. *Phys Rev Lett* 108(10).

166. Feynman RP & Hibbs AR (1965) *Quantum mechanics and path integrals* (McGraw-Hill, New York,) pp xiv, 365 p.
167. Feynman RP (1948) Space-Time Approach to Non-Relativistic Quantum Mechanics. *Rev Mod Phys* 20(2):367-387.
168. Ceperley DM (1995) Path-Integrals in the Theory of Condensed Helium. *Rev Mod Phys* 67(2):279-355.
169. Pollock EL & Ceperley DM (1984) Simulation of Quantum Many-Body Systems by Path-Integral Methods. *Phys Rev B* 30(5):2555-2568.
170. Chandler D & Wolynes PG (1981) Exploiting the Isomorphism between Quantum-Theory and Classical Statistical-Mechanics of Polyatomic Fluids. *J Chem Phys* 74(7):4078-4095.
171. Parrinello M & Rahman A (1984) Study of an F-Center in Molten Kcl. *J Chem Phys* 80(2):860-867.
172. Gillan MJ (1987) Quantum Classical Crossover of the Transition Rate in the Damped Double Well. *J Phys C Solid State* 20(24):3621-3641.
173. Tuckerman ME, Berne BJ, Martyna GJ, & Klein ML (1993) Efficient Molecular-Dynamics and Hybrid Monte-Carlo Algorithms for Path-Integrals. *J Chem Phys* 99(4):2796-2808.
174. Cao JS & Voth GA (1994) The Formulation of Quantum-Statistical Mechanics Based on the Feynman Path Centroid Density .4. Algorithms for Centroid Molecular-Dynamics. *J Chem Phys* 101(7):6168-6183.
175. Horke DA, Chang YP, Dlugolecki K, & Kupper J (2014) Separating Para and Ortho Water. *Angew Chem Int Edit* 53(44):11965-11968.
176. Ceperley DM (1995) *Quantum Monte Carlo Methods for Fermions, pg 427. in The Proceedings of the Les Houches Summer School, Session 56, Strongly Interacting Fermions and High Tc Superconductivity* (Elsevier).
177. Trotter HF (1959) On the product of semi-groups of operators. *Proc. Amer. Math. Soc.* 10(4):545-551.
178. Stern HA & Berne BJ (2001) Quantum effects in liquid water: Path-integral simulations of a flexible and polarizable ab initio model. *J Chem Phys* 115(16):7622-7628.
179. Shiga M & Shinoda W (2005) Calculation of heat capacities of light and heavy water by path-integral molecular dynamics. *J Chem Phys* 123(13).
180. Shinoda W & Shiga M (2005) Quantum simulation of the heat capacity of water. *Phys Rev E* 71(4).
181. Chin SA (2006) A fundamental theorem on the structure of symplectic integrators. *Phys Lett A* 354(5-6):373-376.
182. Chin SA (1997) Symplectic integrators from composite operator factorizations. *Phys Lett A* 226(6):344-348.
183. Suzuki M (1995) Hybrid Exponential Product-Formulas for Unbounded Operators with Possible Applications to Monte-Carlo Simulations. *Phys Lett A* 201(5-6):425-428.
184. Li XP & Broughton JQ (1987) High-Order Correction to the Trotter Expansion for Use in Computer-Simulation. *J Chem Phys* 86(9):5094-5100.
185. Takahashi M & Imada M (1984) Monte-Carlo Calculation of Quantum-Systems .2. Higher-Order Correction. *J Phys Soc Jpn* 53(11):3765-3769.

186. Jang SJ, Jang SM, & Voth GA (2001) Applications of higher order composite factorization schemes in imaginary time path integral simulations. *J Chem Phys* 115(17):7832-7842.
187. Yamamoto TM (2005) Path-integral virial estimator based on the scaling of fluctuation coordinates: Application to quantum clusters with fourth-order propagators. *J Chem Phys* 123(10).
188. Ceriotti M, Brain GAR, Riordan O, & Manolopoulos DE (2012) The inefficiency of re-weighted sampling and the curse of system size in high-order path integration. *P Roy Soc a-Math Phy* 468(2137):2-17.
189. Ceriotti M, Bussi G, & Parrinello M (2010) Colored-Noise Thermostats a la Carte. *J Chem Theory Comput* 6(4):1170-1180.
190. Ceriotti M, Bussi G, & Parrinello M (2009) Langevin Equation with Colored Noise for Constant-Temperature Molecular Dynamics Simulations. *Phys Rev Lett* 102(2).
191. Ceriotti M, Bussi G, & Parrinello M (2009) Nuclear Quantum Effects in Solids Using a Colored-Noise Thermostat. *Phys Rev Lett* 103(3).
192. Dammak H, Chalopin Y, Laroche M, Hayoun M, & Greffet JJ (2009) Quantum Thermal Bath for Molecular Dynamics Simulation. *Phys Rev Lett* 103(19).
193. Tuckerman M, Berne BJ, & Martyna GJ (1992) Reversible Multiple Time Scale Molecular-Dynamics. *J Chem Phys* 97(3):1990-2001.
194. Ceriotti M, More J, & Manolopoulos DE (2014) i-PI: A Python interface for ab initio path integral molecular dynamics simulations. *Comput Phys Commun* 185(3):1019-1026.
195. Eastman P, *et al.* (2013) OpenMM 4: A Reusable, Extensible, Hardware Independent Library for High Performance Molecular Simulation. *J Chem Theory Comput* 9(1):461-469.
196. Eastman P & Pande VS (2010) OpenMM: A Hardware-Independent Framework for Molecular Simulations. *Comput Sci Eng* 12(4):34-39.
197. Kapil V, VandeVondele J, & Ceriotti M (2016) Accurate molecular dynamics and nuclear quantum effects at low cost by multiple steps in real and imaginary time: Using density functional theory to accelerate wavefunction methods. *The Journal of Chemical Physics* 144(5):054111.
198. Wigner E (1932) On the quantum correction for thermodynamic equilibrium. *Phys Rev* 40(5):0749-0759.
199. Kirkwood JG (1934) Quantum statistics of almost classical assemblies. *Phys Rev* 45(2):0116-0117.
200. Feynman RP (1972) *Statistical mechanics; a set of lectures* (W. A. Benjamin, Reading, Mass.,) pp xii, 354 p.
201. Poltavsky I & Tkatchenko A (2016) Modeling quantum nuclei with perturbed path integral molecular dynamics. *Chem Sci* 7(2):1368-1372.
202. DiStasio RA, Santra B, Li ZF, Wu XF, & Car R (2014) The individual and collective effects of exact exchange and dispersion interactions on the ab initio structure of liquid water. *J Chem Phys* 141(8).
203. de la Pena LH & Kusalik PG (2005) Temperature dependence of quantum effects in liquid water. *J Am Chem Soc* 127(14):5246-5251.
204. Vendrell O, Gatti F, Lauvergnat D, & Meyer HD (2007) Full-dimensional (15-dimensional) quantum-dynamical simulation of the protonated water dimer. I. Hamiltonian setup and analysis of the ground vibrational state. *J Chem Phys* 127(18).

205. Vendrell O, Gatti F, & Meyer HD (2007) Full dimensional (15-dimensional) quantum-dynamical simulation of the protonated water dimer. II. Infrared spectrum and vibrational dynamics. *J Chem Phys* 127(18).
206. Richardson JO, Althorpe SC, & Wales DJ (2011) Instanton calculations of tunneling splittings for water dimer and trimer. *J Chem Phys* 135(12).
207. Mukamel S (1995) *Principles of nonlinear optical spectroscopy* (Oxford University Press, New York) pp xviii, 543 p.
208. Lawrence CP & Skinner JL (2002) Vibrational spectroscopy of HOD in liquid D2O. II. Infrared line shapes and vibrational Stokes shift. *J Chem Phys* 117(19):8847-8854.
209. Auer B, Kumar R, Schmidt JR, & Skinner JL (2007) Hydrogen bonding and Raman, IR, and 2D-IR spectroscopy of dilute HOD in liquid D2O. *P Natl Acad Sci USA* 104(36):14215-14220.
210. Wang YM & Bowman JM (2012) Coupled-monomers in molecular assemblies: Theory and application to the water tetramer, pentamer, and ring hexamer. *J Chem Phys* 136(14).
211. Wang YM & Bowman JM (2011) Ab initio potential and dipole moment surfaces for water. II. Local-monomer calculations of the infrared spectra of water clusters. *J Chem Phys* 134(15).
212. Liu J & Miller WH (2007) Linearized semiclassical initial value time correlation functions using the thermal Gaussian approximation: Applications to condensed phase systems. *J Chem Phys* 127(11).
213. Sun X, Wang HB, & Miller WH (1998) Semiclassical theory of electronically nonadiabatic dynamics: Results of a linearized approximation to the initial value representation. *J Chem Phys* 109(17):7064-7074.
214. Sun X, Wang HB, & Miller WH (1998) On the semiclassical description of quantum coherence in thermal rate constants. *J Chem Phys* 109(11):4190-4200.
215. Wang HB, Sun X, & Miller WH (1998) Semiclassical approximations for the calculation of thermal rate constants for chemical reactions in complex molecular systems. *J Chem Phys* 108(23):9726-9736.
216. Habershon S & Manolopoulos DE (2009) Zero point energy leakage in condensed phase dynamics: An assessment of quantum simulation methods for liquid water. *J Chem Phys* 131(24).
217. Hele TJH, Willatt MJ, Muolo A, & Althorpe SC (2015) Communication: Relation of centroid molecular dynamics and ring-polymer molecular dynamics to exact quantum dynamics. *J Chem Phys* 142(19).
218. Hele TJH, Willatt MJ, Muolo A, & Althorpe SC (2015) Boltzmann-conserving classical dynamics in quantum time-correlation functions: "Matsubara dynamics". *J Chem Phys* 142(13).
219. Craig IR & Manolopoulos DE (2005) Chemical reaction rates from ring polymer molecular dynamics. *J Chem Phys* 122(8).
220. Craig IR & Manolopoulos DE (2004) Quantum statistics and classical mechanics: Real time correlation functions from ring polymer molecular dynamics. *J Chem Phys* 121(8):3368-3373.
221. Braams BJ & Manolopoulos DE (2006) On the short-time limit of ring polymer molecular dynamics. *J Chem Phys* 125(12).

222. Cao JS & Voth GA (1994) The Formulation of Quantum-Statistical Mechanics Based on the Feynman Path Centroid Density .2. Dynamical Properties. *J Chem Phys* 100(7):5106-5117.
223. Cao JS & Voth GA (1994) The Formulation of Quantum-Statistical Mechanics Based on the Feynman Path Centroid Density .1. Equilibrium Properties. *J Chem Phys* 100(7):5093-5105.
224. Jang S & Voth GA (1999) A derivation of centroid molecular dynamics and other approximate time evolution methods for path integral centroid variables. *J Chem Phys* 111(6):2371-2384.
225. Hele TJH & Althorpe SC (2013) Derivation of a true (t -> 0(+)) quantum transition-state theory. I. Uniqueness and equivalence to ring-polymer molecular dynamics transition-state-theory. *J Chem Phys* 138(8).
226. Jang S, Sinitskiy AV, & Voth GA (2014) Can the ring polymer molecular dynamics method be interpreted as real time quantum dynamics? *J Chem Phys* 140(15).
227. Miller TF & Manolopoulos DE (2005) Quantum diffusion in liquid water from ring polymer molecular dynamics. *J Chem Phys* 123(15).
228. Rossi M, Liu HC, Paesani F, Bowman J, & Ceriotti M (2014) Communication: On the consistency of approximate quantum dynamics simulation methods for vibrational spectra in the condensed phase. *J Chem Phys* 141(18).
229. Ivanov SD, Witt A, Shiga M, & Marx D (2010) Communications: On artificial frequency shifts in infrared spectra obtained from centroid molecular dynamics: Quantum liquid water. *J Chem Phys* 132(3).
230. Witt A, Ivanov SD, Shiga M, Forbert H, & Marx D (2009) On the applicability of centroid and ring polymer path integral molecular dynamics for vibrational spectroscopy. *J Chem Phys* 130(19).
231. Habershon S, Fanourgakis GS, & Manolopoulos DE (2008) Comparison of path integral molecular dynamics methods for the infrared absorption spectrum of liquid water. *J Chem Phys* 129(7).
232. Reichman DR, Roy PN, Jang S, & Voth GA (2000) A Feynman path centroid dynamics approach for the computation of time correlation functions involving nonlinear operators. *J Chem Phys* 113(3):919-929.
233. Paesani F, Xantheas SS, & Voth GA (2009) Infrared Spectroscopy and Hydrogen-Bond Dynamics of Liquid Water from Centroid Molecular Dynamics with an Ab Initio-Based Force Field. *J Phys Chem B* 113(39):13118-13130.
234. Krishna V & Voth GA (2006) Evaluation of nonlinear quantum time correlation functions within the centroid dynamics formulation. *J Phys Chem B* 110(38):18953-18957.
235. Perez A, Tuckerman ME, & Muser MH (2009) A comparative study of the centroid and ring-polymer molecular dynamics methods for approximating quantum time correlation functions from path integrals. *J Chem Phys* 130(18).
236. Rossi M, Ceriotti M, & Manolopoulos DE (2014) How to remove the spurious resonances from ring polymer molecular dynamics. *J Chem Phys* 140(23).
237. Case DA, *et al.* (2012) AMBER 12. (University of California, San Francisco).
238. Andreoni W & Curioni A (2000) New advances in chemistry and materials science with CPMD and parallel computing. *Parallel Comput* 26(7-8):819-842.

239. Blum V, *et al.* (2009) Ab initio molecular simulations with numeric atom-centered orbitals. *Comput Phys Commun* 180(11):2175-2196.
240. Clark SJ, *et al.* (2005) First principles methods using CASTEP. *Z Kristallogr* 220(5-6):567-570.
241. VandeVondele J, *et al.* (2005) QUICKSTEP: Fast and accurate density functional calculations using a mixed Gaussian and plane waves approach. *Comput Phys Commun* 167(2):103-128.
242. Bohm E, *et al.* (2008) Fine-grained parallelization of the Car-Parrinello ab initio molecular dynamics method on the IBM Blue Gene/L supercomputer. *Ibm J Res Dev* 52(1-2):159-175.
243. Tuckerman ME, Yarne DA, Samuelson SO, Hughes AL, & Martyna GJ (2000) Exploiting multiple levels of parallelism in Molecular Dynamics based calculations via modern techniques and software paradigms on distributed memory computers. *Comput Phys Commun* 128(1-2):333-376.
244. Markland TE, *et al.* (2012) Theory and simulations of quantum glass forming liquids. *J Chem Phys* 136(7).
245. Markland TE, *et al.* (2011) Quantum fluctuations can promote or inhibit glass formation. *Nat Phys* 7(2):134-137.
246. Zhang C, Donadio D, Gygi F, & Galli G (2011) First Principles Simulations of the Infrared Spectrum of Liquid Water Using Hybrid Density Functionals. *J Chem Theory Comput* 7(5):1443-1449.
247. Guidon M, Hutter J, & VandeVondele J (2010) Auxiliary Density Matrix Methods for Hartree-Fock Exchange Calculations. *J Chem Theory Comput* 6(8):2348-2364.
248. Grimme S (2011) Density functional theory with London dispersion corrections. *Wires Comput Mol Sci* 1(2):211-228.
249. Reilly AM & Tkatchenko A (2015) van der Waals dispersion interactions in molecular materials: beyond pairwise additivity. *Chem Sci* 6(6):3289-3301.
250. DiLabio GA, Johnson ER, & Otero-de-la-Roza A (2013) Performance of conventional and dispersion-corrected density-functional theory methods for hydrogen bonding interaction energies. *Phys Chem Chem Phys* 15(31):12821-12828.
251. Del Ben M, Hutter J, & VandeVondele J (2015) Probing the structural and dynamical properties of liquid water with models including non-local electron correlation. *J Chem Phys* 143(5).
252. Hohenstein EG, Parrish RM, & Martinez TJ (2012) Tensor hypercontraction density fitting. I. Quartic scaling second- and third-order Moller-Plesset perturbation theory. *J Chem Phys* 137(4).
253. Spura T, Elgabarty H, & Kuhne TD (2015) "On-the-fly" coupled cluster path-integral molecular dynamics: impact of nuclear quantum effects on the protonated water dimer (vol 17, pg 14355, 2015). *Phys Chem Chem Phys* 17(29):19673-19674.
254. Zen A, Luo Y, Mazzola G, Guidoni L, & Sorella S (2015) Ab initio molecular dynamics simulation of liquid water by quantum Monte Carlo. *J Chem Phys* 142(14).
255. Babin V, Leforestier C, & Paesani F (2014) Development of a "First-Principles" Water Potential with Flexible Monomers: Dimer Potential Energy Surface, VRT Spectrum, and Second Virial Coefficient (vol 9, pg 5395, 2013). *J Chem Theory Comput* 10(5):2212-2212.

256. Babin V, Medders GR, & Paesani F (2014) Development of a "First Principles" Water Potential with Flexible Monomers. II: Trimer Potential Energy Surface, Third Virial Coefficient, and Small Clusters. *J Chem Theory Comput* 10(4):1599-1607.
257. Babin V, Leforestier C, & Paesani F (2013) Development of a "First Principles" Water Potential with Flexible Monomers: Dimer Potential Energy Surface, VRT Spectrum, and Second Virial Coefficient. *J Chem Theory Comput* 9(12):5395-5403.
258. Luehr N, Ufimtsev IS, & Martinez TJ (2011) Dynamic Precision for Electron Repulsion Integral Evaluation on Graphical Processing Units (GPUs). *J Chem Theory Comput* 7(4):949-954.
259. Ufimtsev IS & Martinez TJ (2009) Quantum Chemistry on Graphical Processing Units. 3. Analytical Energy Gradients, Geometry Optimization, and First Principles Molecular Dynamics. *J Chem Theory Comput* 5(10):2619-2628.
260. Ufimtsev IS & Martinez TJ (2008) Graphical Processing Units for Quantum Chemistry. *Comput Sci Eng* 10(6):26-34.
261. Smith KKG, Poulsen JA, Nyman G, & Rossky PJ (2015) A new class of ensemble conserving algorithms for approximate quantum dynamics: Theoretical formulation and model problems. *J Chem Phys* 142(24).
262. Liu J (2014) Path integral Liouville dynamics for thermal equilibrium systems. *J Chem Phys* 140(22).
263. Maksyutenko P, Rizzo TR, & Boyarkin OV (2006) A direct measurement of the dissociation energy of water. *J Chem Phys* 125(18).
264. Dyke TR & Muenter JS (1973) Electric Dipole-Moments of Low J States of H2o and D2o. *J Chem Phys* 59(6):3125-3127.
265. Ch'ng LC, Samanta AK, Czako G, Bowman JM, & Reisler H (2012) Experimental and Theoretical Investigations of Energy Transfer and Hydrogen-Bond Breaking in the Water Dimer. *J Am Chem Soc* 134(37):15430-15435.
266. Rocher-Casterline BE, Mollner AK, Ch'ng LC, & Reisler H (2011) Imaging H2O Photofragments in the Predissociation of the HCl-H2O Hydrogen-Bonded Dimer. *J Phys Chem A* 115(25):6903-6909.
267. Rocher-Casterline BE, Ch'ng LC, Mollner AK, & Reisler H (2011) Communication: Determination of the bond dissociation energy (D-0) of the water dimer, (H2O)(2), by velocity map imaging. *J Chem Phys* 134(21).
268. Hill PG, Macmillan RDC, & Lee V (1982) A Fundamental Equation of State for Heavy-Water. *J Phys Chem Ref Data* 11(1):1-14.
269. Kudish AI, Steckel F, & Wolf D (1972) Physical Properties of Heavy-Oxygen Water - Absolute Viscosity of H2o-18 between 15 and 35 Degrees C. *J Chem Soc Farad T 1* 68(11):2041-&.
270. Kell GS (1977) Effects of Isotopic Composition, Temperature, Pressure, and Dissolved-Gases on Density of Liquid Water. *J Phys Chem Ref Data* 6(4):1109-1131.
271. Nakamura M, Tamura K, & Murakami S (1995) Isotope Effects on Thermodynamic Properties - Mixtures of X(D2o or H2o)+(1-X)Ch3cn at 298.15 K. *Thermochim Acta* 253:127-136.
272. Holz M, Heil SR, & Sacco A (2000) Temperature-dependent self-diffusion coefficients of water and six selected molecular liquids for calibration in accurate H-1 NMR PFG measurements. *Phys Chem Chem Phys* 2(20):4740-4742.

273. Price WS, Ide H, Arata Y, & Soderman O (2000) Temperature dependence of the self-diffusion of supercooled heavy water to 244 K. *J Phys Chem B* 104(25):5874-5876.
274. Harris KR & Woolf LA (1980) Pressure and Temperature-Dependence of the Self-Diffusion Coefficient of Water and O-18 Water. *J Chem Soc Farad T 1* 76:377-385.
275. Hardy EH, Zygar A, Zeidler MD, Holz M, & Sacher FD (2001) Isotope effect on the translational and rotational motion in liquid water and ammonia. *J Chem Phys* 114(7):3174-3181.
276. Eisenberg DS & Kauzmann W (1969) *The structure and properties of water* (Clarendon P., Oxford,) pp xii, 296, (293) p.
277. Horita J & Wesolowski DJ (1994) Liquid-Vapor Fractionation of Oxygen and Hydrogen Isotopes of Water from the Freezing to the Critical-Temperature. *Geochim Cosmochim Ac* 58(16):3425-3437.